Variability in the X-Ray Emission of H0538+608, An Unusual AM Her-type Cataclysmic Variable

by

Jennifer Catelli

Submitted to the Department of Physics
on May 8, 1992, in partial fulfillment of the
requirements for the degree of
Bachelor of Science in Physics

Abstract

The X-ray emissions of AM Herculis-type object H0538+608 were observed using the ROSAT satellite. Evidence was found for a highly varying soft X-ray component with a much lower intensity than is typical for this class. The spectrum was well fit by a thermal brehmsstrahlung model (exponential plus gaunt factor) of 35 ±5 KeV plus a 0.05 ±0.01 KeV blackbody component, with absorption by interstellar medium with a neutral hydrogen column density of $\log N_H(\text{atoms/cm}^2)=20.2$. No obvious periodic variations were found. There was very little correlation between the hard and soft X-ray bands.

Thesis Supervisor: Alan Levine
Title: Research Scientist

Variability in the X-Ray Emission of H0538+608, An Unusual AM Her-type Cataclysmic Variable

by

Jennifer Catelli

Submitted to the Department of Physics
in partial fulfillment of the requirements for the degree of

Bachelor of Science in Physics

at the

MASSACHUSETTS INSTITUTE OF TECHNOLOGY

May 1992

Author ..... Jennifer R. Catelli
Department of Physics
May 8, 1992

Certified by ..... Alan M Levine
Alan Levine
Research Scientist
Thesis Supervisor

Accepted by .....
Aaron Bernstein
Chairman, Departmental Committee

Acknowledgments

I would like to thank Derrick Kong for answering questions about obscure computer functions at 4 in the morning. I would also like to thank my supervisor, Al Levine, for his help and advice, David Buote, for getting me started on IRAF, and Andy Silber, for letting me use his programs and giving helpful comments about H0538+608.

Variability in the X-Ray Emission of H0538+608, An Unusual AM Her-type Cataclysmic Variable

by

Jennifer Catelli

Submitted to the Department of Physics
on May 8, 1992, in partial fulfillment of the
requirements for the degree of
Bachelor of Science in Physics

Abstract

The X-ray emissions of AM Herculis-type object H0538+608 were observed using the ROSAT satellite. Evidence was found for a highly varying soft X-ray component with a much lower intensity than is typical for this class. The spectrum was well fit by a thermal brehmsstrahlung model (exponential plus gaunt factor) of 35 $\pm$5 KeV plus a 0.05 $\pm$0.01 KeV blackbody component, with absorption by interstellar medium with a neutral hydrogen column density of $\log N_H(\text{atoms/cm}^2)$=20.2. No obvious periodic variations were found. There was very little correlation between the hard and soft X-ray bands.

Thesis Supervisor: Alan Levine
Title: Research Scientist

Contents

Chapter 1

Introduction

A binary star system in which a white dwarf is accreting matter from a late-type companion is known as a cataclysmic variable. AM Herculis-type cataclysmic variables are a subclass of these objects in which the white dwarf has a strong magnetic field (greater than 10^7 Gauss). The magnetic field has drastic effects on the dynamics of such systems, giving AM Her objects a number of distinctive characteristics.

The magnetic field of the white dwarf controls the accretion path from the inner Lagrangian point to either one or both of the magnetic poles of the white dwarf, causing the mass transfer to occur as a stream instead of through an accretion disk, in which the mass could spiral towards the surface more slowly. This lack of an accretion disk means that changes in the mass flow have immediate and strong effects on the luminosity of the object. The accretion stream forms a standing shock near the surface of the white dwarf (See Figure 1.1), which becomes the source of most of the high-energy emissions. [5]

The principal identifying feature of an AM Her system is the high degree of both linear and circular polarization at optical frequencies; this feature prompted the suggestion of the name 'polars' for the class. The circular polarization, from cyclotron radiation of semi-relativistic electrons in the magnetic field of the white dwarf, can exceed 10%. [4]

There is considerable evidence for precise spin-orbit synchronization in these systems. This synchronization is thought to be due to the dipole-dipole interactions of

the two stars, and to develop on a short timescale relative to the evolution of the system because of the magnetic field strength. Typical orbital periods range from one to four hours. Essentially all of the emissions are modulated by this linked spin and orbital period. [4]

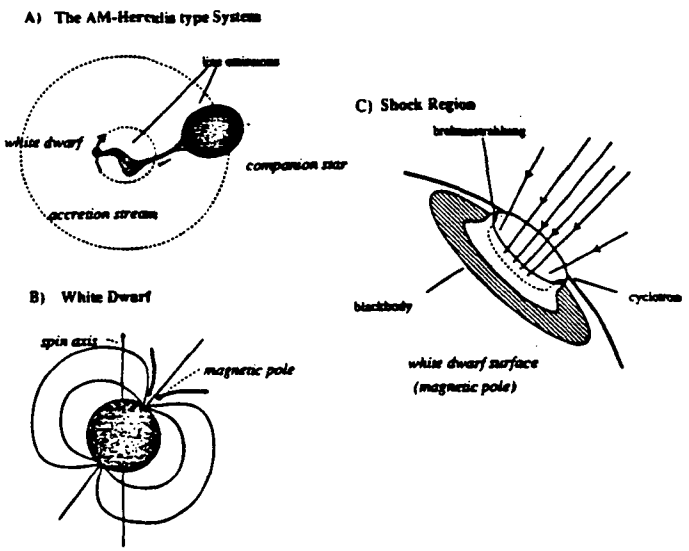

Figure 1.1 – (based on Liebert, 1985) The believed structure of an AM Herculis type system is shown, with locations of emissions marked. Three views are given: A) the entire system; the two dashed circles are the orbits of the two stars about their center of mass, B) the white dwarf itself, and C) the shock region near the magnetic pole of the white dwarf, where the majority of the high energy emissions arise.

According to the standard model, the X-ray emissions consist of two main components: a soft X-ray/EUV blackbody component from the white dwarf surface and a hard thermal brehmsstrahlung component from the postshock region. The blackbody emission may be due to the heating of the white dwarf by the the hard X-ray and optical emissions. Roughly half of the brehmsstrahlung and cyclotron emissions are radiated away from the white dwarf, becoming the hard X-ray and optical components, respectively. The other half of this radiation hits the white dwarf, heating the surface and being re-emitted as the soft X-ray blackbody component. This implies that the luminosities of these two components should be comparable: $L_{bb} \simeq (L_{cyc} + L_{bre})$. Instead, there is an excess of power in the soft X-ray region which has not yet been satisfactorily explained, so that $L_{bb} \geq 50 \times (L_{cyc} + L_{bre})$. This phenomenon is known

as the 'soft excess problem'. The face of the companion star is also heated by the emissions of the shock region and by the blackbody radiation, giving rise to intense H, He I, and He II emission lines.[4]

H0538+608 was detected by the HEAO-1 and Uhuru satellite surveys, and was identified as an AM Her by Remillard et al. [8] on the basis of its optical spectrum. The object displayed all of the optical characteristics typical of the class: intense emission lines, circular polarization, and strong brightness variations.

Observations with the IUE satellite showed H0538+608 to have an unusual UV spectrum. The spectrum was dominated by the N V line, and had a very weak C IV line, giving a nitrogen/carbon ratio approximately 20 times greater than is generally found. The unusual chemical abundances resembled those seen in some post-nova systems. Bonnet-Bidaud and Mouchet hypothesized that it either was a post-nova system or had an unusual companion star.[2]

Simultaneous IUE, EXOSAT, and optical telescope observations by Schraeder et al. further established H0538+608 as an unusual object. The intensity of the emission lines varied, there was an unusually high X-ray to optical luminosity ratio, and erratic X-ray light curves. Strong eclipse-like features were found in the soft X-ray band which were not apparent in the other bands. The soft excess seemed not to be present. They also found evidence indicating that the spin-orbit synchronization might be missing, but it was such that the variations might also be explained by uneven mass accretion.[9]

A two year program of optical spectroscopy, photometry, and polarimetry was undertaken by Mason, Liebert, and Schmidt. A precise period of 3.322171 ± 0.000014 hours was determined by polarimetry, but labelled "tentative" because spikes were not always visible when expected. The cyclotron emissions came in both polarizations, and varied in relative intensity. This led to a model for the system with accretion spots at both magnetic poles, one of which was eclipsing while the other always remained in view. The possibility of asynchronous rotation was once again considered and, although it was concluded at this point that there was no concrete evidence for such, the possibility was left open.[6]

Ginga satellite data gave evidence that there were two distinct states of the system, a pulsed state and a flaring state, and that the object switched between the two every few days. The pulsing state was modulated by a 3.3 hr period, showing eclipse like features in the soft X-ray region. The flaring state was not modulated at this period. The system was once again modelled with two accretion points, one eclipsing, one not, with the eclipsing point not accreting during the flaring state. The high energy X-ray emissions from the standing shock region were found to correspond well with a thin thermal emission (brehmsstralung) plus an iron K-line. The temperature in the pulsing state was found to change with the spin phase, while the temperature in the flaring state correlated with source luminosity. [3]

Optical observations undertaken at the same time as the *Ginga* observations showed evidence for a possible 1.3% difference in the spin and rotational periods of the system. The change in accretion geometry which occured during the observations was linked to states caused by asynchronous rotation.[10]

This indicates a possible link with the only other known asynchronous AM Her, V1500 Cygni, the remnant of Nova Cygni 1975, which apparently had its synchronization disturbed by the nova event. The pre-nova system was a synchronized AM Her, and the post-nova system has a 1.8% difference in the spin and orbit periods.[12] An extensive search of the past 100 years of Harvard College Observatory Plate Stacks (1200 plates) was conducted looking for a nova near H0538+608, but none was found.[8] This is not conclusive evidence in either direction, since the period of time spanned by these plates was not large enough to rule the possibility out, and no evidence of a nova event was discovered.

In an attempt to gain more information about this unusual object, H0538+608 was observed with the ROSAT satellite in March of 1991. In this paper I will present these results and discuss the system based on these observations.

Chapter 2

Observations

The ROSAT observations of H0538+608 took place over a five day period, from March 9 to 14, 1991. The observations were divided into 14 observation intervals (OBIs), which varied in duration from 882 to 2299 seconds. The net observation time was 19209 seconds. H0538+608 was much brighter than anything else in the field of view (see Figure 2.1).

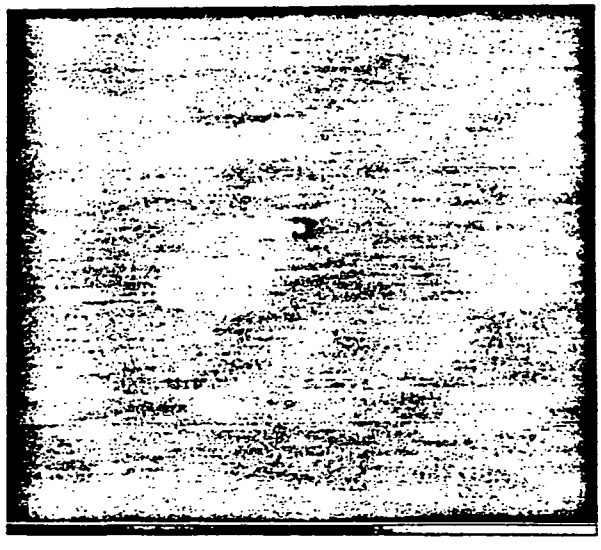

Figure 2.1 – A gray-scale image of the PSPC field of view. H0538+608 is the bright source in the center.

ROSAT is an acronym for Röntgensatellit, a joint German, US, and British space project. The main instrument on the satellite is an X-ray telescope with a grazing incidence mirror configuration. A schematic of the telescope is shown in Figure 2.2.

The focal length of the telescope is 240 cm, and there are two position sensitive proportional counters (PSPCs) in the focal plane to the telescope, as well as a high resolution imager.

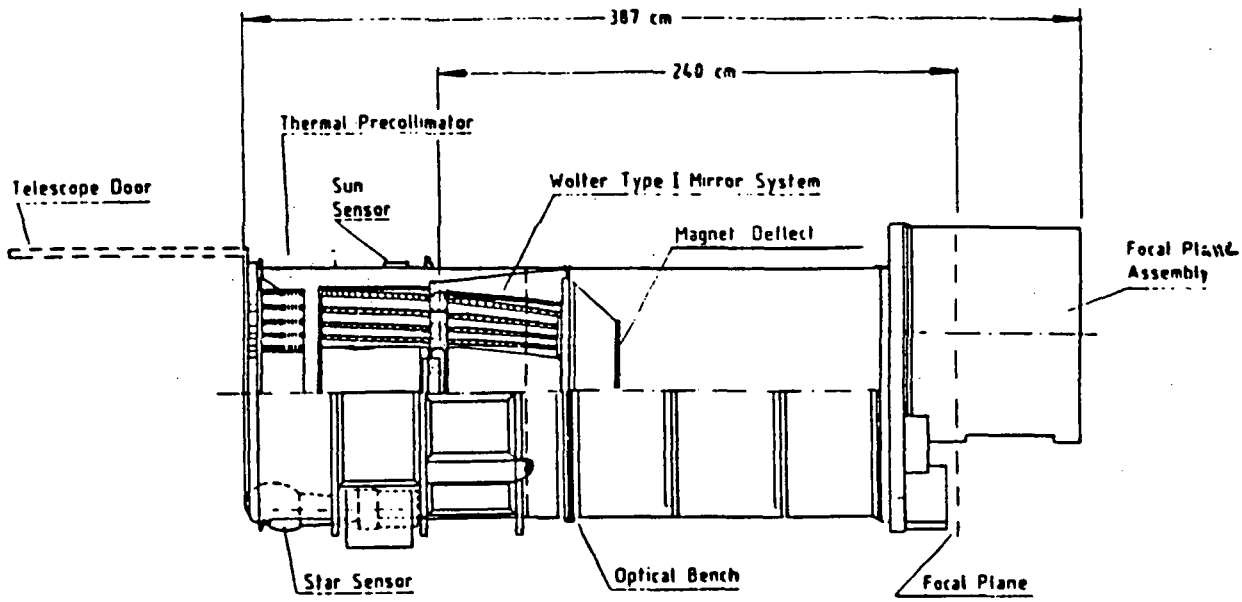

Figure 2.2 – (from the ROSAT mission description) A schematic of the ROSAT X-ray telescope and its major components. The focal plane turret contains two PSPCs and the high-resolution imager.

The satellite is in low earth orbit and therefore has a number of restrictions on viewing time, the principal ones being earth occultation and passage through regions of enhanced energetic charged particle density. The earth subtends about 136° of the satellite's field of view, occulting a large segment of the sky. The high energetic charged particle densities in the northern and southern auroral belts and the South Atlantic Anomaly regions interfere with the operation of electronics in those regions and therefore prevent data being taken; this constraint prevents the use of the telescope about 27% of the time. These, along with a number of other constraints, limit the viewing of most sources to short duration intervals, spread over a large segment of time. In general, viewing intervals with ROSAT are less than 4000 seconds in length.

The H0538+608 observations were made using one of the PSPCs. The PSPC has an energy range of 0.1 to 2 KeV, and a time resolution of 130 microseconds, and records the event time, pulse height, and position for each event. It has a circular field of view 2° in diameter. The PSPC window is made of 1 μm polypropylene foil, with

a coating of 50 μg cm^{-2} carbon and 40 μg cm^{-2} lexan to prevent UV radiation from interfering with the X-ray data. These coatings, together with the polypropylene, make the window basically opaque just above the carbon edge at 0.28 KeV, however. The quantum efficiency of the detector is given in Figure 2.3.

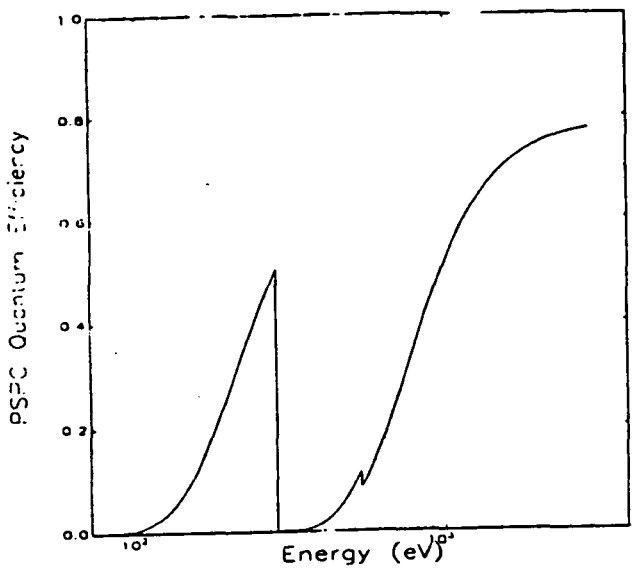

Figure 2.3 – (from the ROSAT mission description) The quantum efficiency of the PSPC vs energy.

The window is supported by two layers of wire mesh, one finer than the other, as well as a radial beam support structure. During observations the satellite slowly oscillates back and forth, in what is known as "wobble" mode, to prevent the permanent occultation of a source by a wire. This motion changes the pointing direction by $\pm$ 3 arcmin in 400 seconds.

Chapter 3

Data Analysis and Results

3.1 PROS and the IRAF environment

The majority of the data analysis was done using PROS, Post-Reduction Off-line Software, an X-ray data analysis utility written at the Harvard-Smithsonian Astrophysical Observatory for use with data from the ROSAT and *Einstein* satellites. PROS runs under IRAF, the Image Reduction and Analysis Facility written at the National Optical Astronomy Observatory. PROS has image reduction, timing analysis, and spectral analysis functions, and is organized around the QPOE file structure. QPOE is an acronym for quick position-ordered event files, which are photon lists with arrival time, energy, and position for each photon detected. The headers of these files contain details of the satellite parameters for the specific set of observations, making it possible to correct for many systematic variations. These files can be sorted by energy or time-bin, and then converted into ASCII files for use with analysis routines outside of PROS.

3.2 Light Curves

The complete data set was restricted to a region just around H0538+608. This removed the emissions from the other sources in the PSPC's field of view. This data was then timesorted and binned to form lightcurves which could be tested for

variability. This image and time manipulation was done using PROS, specifically the *timsort* and *ltcurv* subroutines of the *xtiming* package. The lightcurve is shown in Figure 3.1 and, in more detail, in Appendix A.

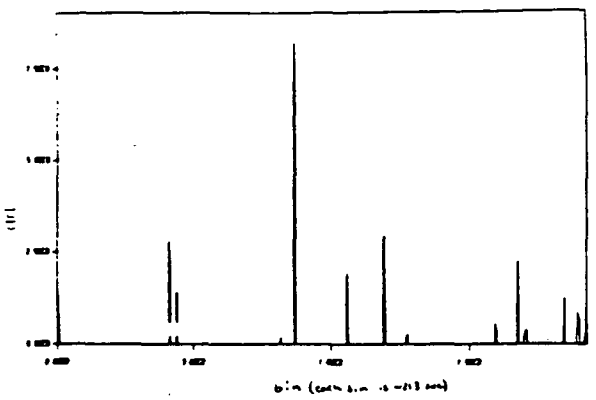

Figure 3.1 – The lightcurve for all of the observation intervals.

The data was further separated into hard and soft X-ray components, the boundary between which was determined by the spectral fit (See Figure 3.4). The two energy bands were chosen so that the counts in the first, PHA[1] bin 7 to 40, corresponded to the blackbody component, and the counts in the second, PHA bin 70 to 240, corresponded to the optically thin thermal brehmsstrahlung component. These lightcurves were then cross-correlated to determine some measure of the interdependance of the emission mechanisms in the two bands. The correlation between two series is defined by:

$$Corr_j(g,h) = \frac{\sum(g_i - \bar{g})(h_{i+j} - \bar{h})}{\sqrt{\sum(g_i - \bar{g})^2 \sum(h_{i+j} - \bar{h})^2}}$$

For the most part it appeared that the hard and soft bands had very little correlation between them, and that the variations with time delay were mostly random. Only in a few instances did the correlation rise above 0.3. The higher correlations appear to correspond to the intervals in which there was a very low count rate. A correlation function typical of most of the intervals is shown in Figure 3.2. The

[1] pulse height analyzer

correlations for all of the intervals, along with their autocorrelations, are shown in Appendix C.

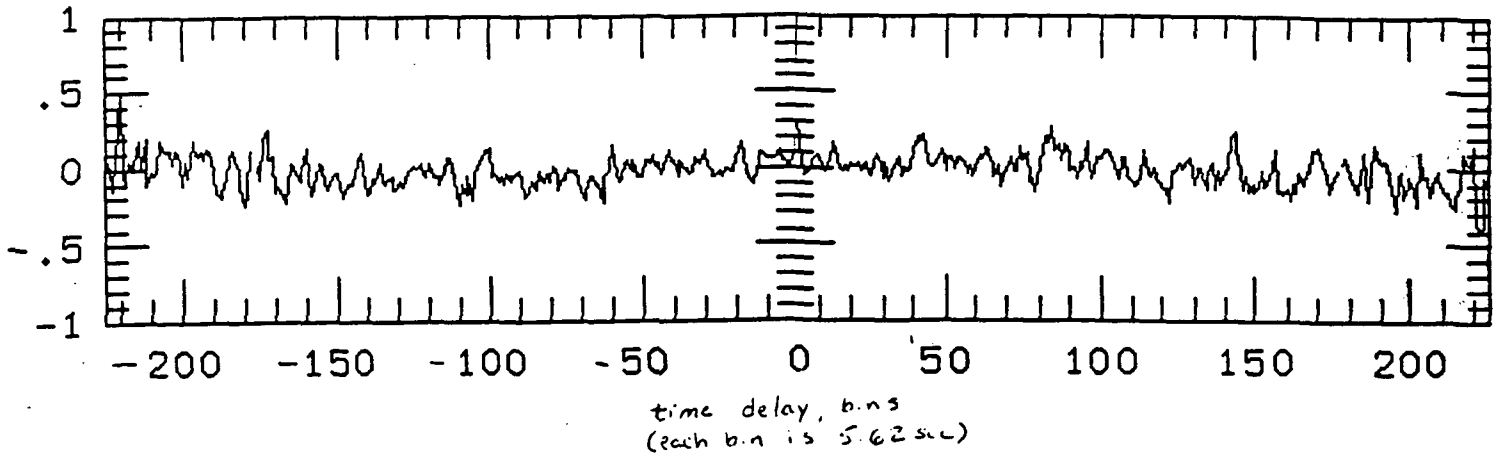

Figure 3.2 – Cross correlation, for a single observation interval(OBI 1).

One of the more interesting time intervals is OBI 5, in which the object shows an extremely high flux, mostly in the soft X-ray region. This variation is significantly larger than all of the other changes, possibly indicating a unique event rather than a periodic variation. This flaring is almost entirely in the soft X-ray band; throughout the observations the variations in the soft X-ray region are much greater than those in the hard X-ray. There are short duration bursts of activity in the soft X-ray band in a number of the OBIs, notably 7 and 10. There are also several OBIs in which the soft component vanishes almost entirely.

3.3 Periodicities

Both the phase dispersion minimization technique developed by Stellingwerf [11] and period folding were used in an attempt to determine the orbital period and other regular variations in the X-ray lightcurves. Phase dispersion minimization is a technique which minimizes the variance with respect to the mean light curve using a least squares approach. This method theoretically deals well with a small number

of irregularly spaced data intervals. The event files used in this were first binned into ten second intervals within PROS, using the *ltcurv* binning routine, and then converted into ASCII files, using *timprint*, before being analysed. [2] Period folding is accomplished by breaking a period of length N into a number of bins, and placing all of the points x(t) from the entire series into this length, in the time bin determined by mod_N(t/bin size). Then a χ^2 test is done on this folded lightcurve to determine how much it varies from a straight line. The greater the variation, the more likely it is that a given period corresponds to a period in the time series. A period search algorithm can be developed from this by allowing the period length N to vary and maximizing χ^2. Period folding was done within PROS using the routine *period* on timesorted event files.

Table 3.2 – Period Searches

Period(sec ±60)	Period(hr ±0.02	χ^2(PDM)	χ^2(PF)
5280	1.47	0.67	1.5×10^6
6960	1.93	0.62	1.6×10^8
7980	2.21	0.55	5.9×10^6
8825	2.45	0.58	1.2×10^7
9840	2.73	0.69	5.5×10^7
10500	2.92	0.58	3.1×10^7
11049	3.06	0.77	9.4×10^6
12000	3.33	0.78	3.3×10^6
13020	3.62	0.65	3.9×10^6
14220	3.95	0.70	3.8×10^6
14640	4.07	0.53	5.9×10^6

Table 3.2 shows the results of the searches conducted to find the orbital period. The data was searched for regular variations from one hour to six hours long. The orbital period was extremely elusive; the large data gaps and the fact that all of the OBIs were considerably shorter than the supposed orbital period caused difficulties in the period search algorithms. The significant peaks for each search method were identified; those listed were found using both methods. The χ^2 columns in the table are not meant to be of great significance, but only to indicate the relative importance

[2] Using a program written by Andy Silber.

of the peaks, according to the period-search algorithms. A high χ^2 is considered a good fit for period folding, while a low χ^2 is good for the phase dispersion technique. One of the possible periods found (3.33 hours = 12000 sec) corresponds to the period found in previous study of H0538+608. However, there is nothing in particular to distinguish this period from the others based solely on these results. In fact, 3.33 hours is one of the least likely of these periods.

The reason that several search algorithms were used is that the initial method, period folding, gave extremely different results when parameters such as the number of bins or the step length were changed. These inconsistent results seemed to imply that many of the peaks found were in fact artifacts of the program, and not true variations in the data. Phase dispersion minimization, which also gave rise to a large number of possible periods, was used to remove some of the artifacts from the folding data. This comparision should have removed most periodicities induced by the search algorithms.

A possible problem with the period searches is that many of the lengths of the observation intervals, and the lengths of the gaps between them are of an order which is comparable to the periodicities being hunted, and therefore can introduce false peaks into the results. There are no clear candidates for periodic variation in the fifteen minute to an hour range, because the OBIs are all between fifteen minutes and 1/2 hour in length, and their lengths dominate searches in this time period, making it very difficult to determine if any given peak is real or not. One regular variation, 10500 seconds is very close to the length of one of the gaps between intervals, which is 10579 seconds long.

Table 3.3 – Short Periodic Variations

(in seconds)

550 ± 5	587 ± 5	627 ± 4	671 ± 4
737 ± 3	766 ± 4	780 ± 3	855 ± 4

Each interval was also searched for variations on a shorter timescale, from one to fifteen minutes. The OBIs were searched individually to avoid the problems with data

gaps. There were no short-time periodicities found in common among all fourteen intervals. Those listed in Table 3.3 were found in at least four of the fourteen OBIs.

Figure 3.3 – Plots of the attempts to determine orbital period: a) period folding, b) phase dispersion minimization, and c) power spectrum.

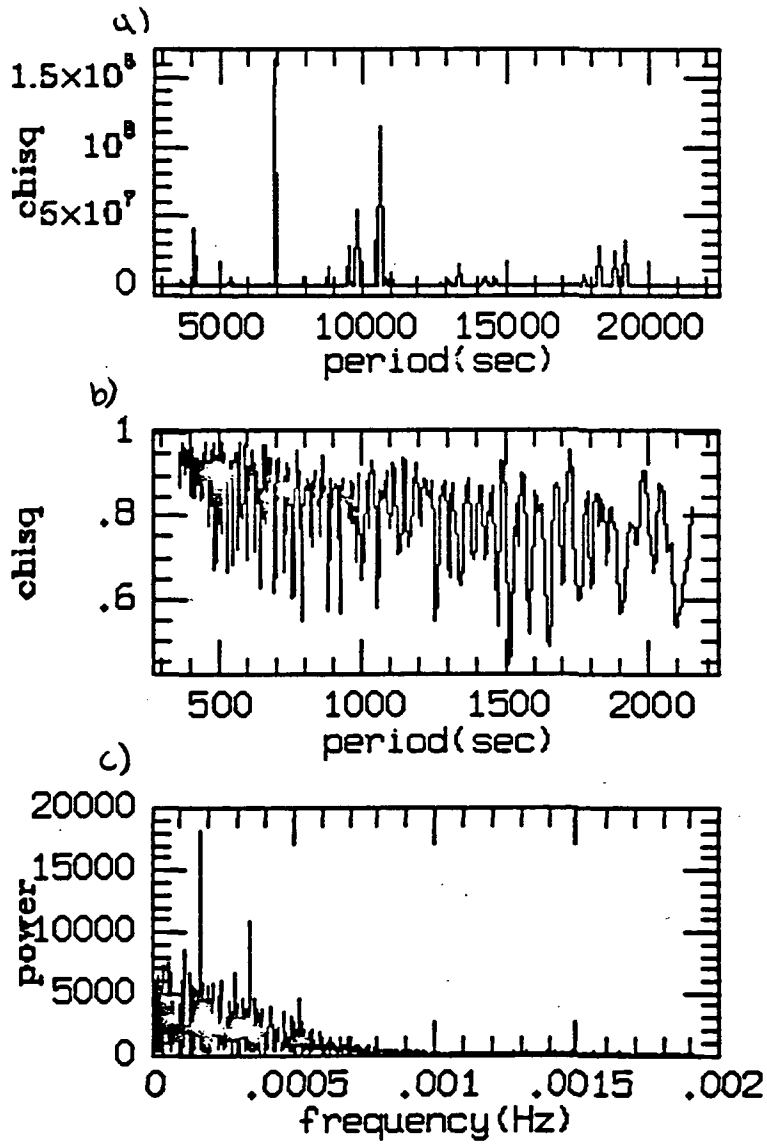

3.4 Spectral Analysis

Using the PROS spectral package, the data was sorted by energy bin, and then fit to various spectral models. The spectra for each of the OBIs was fit to a thermal brehmsstrahlung (exponential plus gaunt) plus soft blackbody model, modified for hydrogen absorption. The model was chosen based on the work done by Ishida [2]. The total spectrum was also fit. The spectra for all of the intervals are shown in Appendix B. Several of these do not have associated best-fit curves plotted, due to an error in the spectral fitting program.

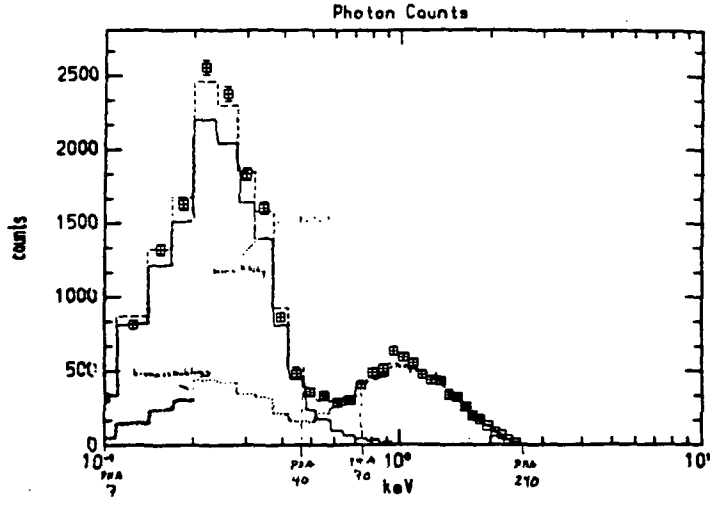

Figure 3.4 – The total spectrum, plotted with the best fit. The contributions of the induvidual components of the spectral model are shown, along with the points at which the data was separated into "hard" and "soft" components.

The total spectrum indicates a good fit with an optically thin hot plasma plus a blackbody component. The overall spectrum is fit by a 35±5 KeV brehmsstrahlung plus 0.05±0.01KeV blackbody component, with a neutral hydrogen column density $\log N_H(\text{atoms/cm}^2) = 20.20$.

Table 3.4 shows the results of the spectral fits done using the PROS Simplex spectral fitting routine. The fluxes given are those measured for the specific component of the spectrum and are in units of ergs/cm^2/s. The energy of the spectral models were integrated from 0.15 KeV to 2 KeV, using the PROS *xflux* routine. The fluxes given in Table 3.5 are in the same units, and are calculations of the flux if the spectral

model is integrated from 0.1 to 100 KeV, instead of being cut off at the PSPC upper limit, and then corrected for absorption. There appears to be some sort of error in the time normalization, as the flux per unit time should not be much greater for the total interval than for the induvidual intervals. This sort of error should not effect comparisons of the two bands, however.

Table 3.4 – Spectral Fits

OBI	reduced χ^2	logNH	bre temp(KeV)	bre flux	bla temp(KeV)	bla flux	total flux
all	3.16	20.20	38.2	4.98×10^{-12}	0.05	2.77×10^{-12}	7.77×10^{-12}
2	1.4	20.31	34.9	5.13×10^{-13}	0.041	3.05×10^{-13}	8.25×10^{-13}
5	1.7	20.21	44.98	2.96×10^{-13}	0.05	1.08×10^{-12}	1.38×10^{-12}
7	1.16	20.23	28.0	7.51×10^{-13}	0.047	2.54×10^{-13}	1.00×10^{-12}
9	1.4	19.739	30.009	2.81×10^{-13}	0.093	1.35×10^{-14}	2.93×10^{-13}
10	1.55	19.153	30.003	6.23×10^{-13}	0.057	6.02×10^{-15}	6.28×10^{-13}
11	1.24	19.844	30.048	2.19×10^{-13}	0.045	5.70×10^{-14}	2.77×10^{-13}
13	2.3	20.34	37.82	5.31×10^{-13}	0.028	1.11×10^{-22}	5.34×10^{-13}

Table 3.5 – Energy Fluxes of Spectral Model Components

OBI	bre flux	bla flux	total flux
all	5.00×10^{-11}	1.00×10^{-11}	6.02×10^{-11}
2	5.04×10^{-12}	1.84×10^{-12}	6.88×10^{-12}
5	3.35×10^{-12}	3.65×10^{-12}	6.77×10^{-12}
7	6.26×10^{-12}	1.06×10^{-12}	7.17×10^{-12}
9	2.28×10^{-12}	1.45×10^{-18}	2.29×10^{-12}
10	4.87×10^{-12}	2.89×10^{-14}	4.88×10^{-12}
11	2.08×10^{-12}	1.35×10^{-18}	2.08×10^{-12}
13	4.97×10^{-12}	8.48×10^{-13}	5.59×10^{-12}

Chapter 4

Discussion and Conclusions

4.1 Period

There was no strong evidence to support any conclusions about the orbital period. A number of possible periodic variations were found, none standing out clearly as the orbital period. The intervals in which the source was being observed were all less than one-fifth the length of the previously reported period of 3.322 hours.[6] These intervals were not only short, but they were also unevenly spaced, with long gaps between them. This combination caused a number of problems with the search algorithms used to determine the period.

The previously reported 3.3 hour period was among the possible periodicities found, but it was one of the least likely. There was a great deal of variation, most of it in the soft X-ray rather than the hard X-ray, but there was no dominant periodicity. The soft X-ray component was very strong in some OBIs and almost completely gone in others. The variations found could correspond with the orbital period of the system, the spin period of the white dwarf, or variations in the mass accretion rate.

4.2 Spectrum

Spectral analysis yielded more definite results than the period searches. Because the period was undetermined, it was difficult to link the changes in the spectra with orbital

phase. It is not even clear if the data breaks into "pulsing" and "flaring" states, as has been proposed. [3] The data fit reasonably well to a thermal brehmsstrahlung of 35 ±5 KeV plus a blackbody component of 0.045 ± 0.01 KeV, with a neutral hydrogen column density $\log N_H$(atoms cm^{-2})= 20.2. From a comparison of the energy fluxes of the different components it can be seen that the soft excess typical of AM Hers is not present in this system. The largest ratio of the soft to hard bands was found during OBI 5, and is approximately 1.09, which does not approach the ratio of 50 found in others of this class.

4.3 Correlation

The correlation between the two selected energy bands was very low. This is a surprising result, because previous study had shown a strong correlation bewteen the optical and hard X-ray bands. This implies that the mechanisms producing the two components are not closely related in time. Only in a few cases did the correlation go above 0.3, and these cases were intervals in which the count rate was extremely low.

The autocorrelation functions all dropped off rapidly with time delay, most dropping to around zero correlation by approximately 30 seconds of lag. OBI 14 shows an unusual autocorrelation in the soft band; it is probably a construct of the program used to correlate the functions, since there is no particularly unusual behavior visible in the light curve for that interval.

4.4 Suggestions for Further Resarch

Further study of H0538+608 could reveal more of how the spectral changes are linked to the variation of the lightcurve. An accurate orbital period could link various parameters to phase, and determine more about the actual structure of the object. The erratic variations in the lightcurve could also be analysed for chaos; the aperiodic appearance of the variations makes chaotic behavior a strong possibility. H0538+608 still has many behavioral peculiarities to be explained.

Appendix A

Light Curves

The following few pages contain the light curves for all of the OBIs. For each interval there are three light curves. The top light curve is total energy, the second is soft energy (pha channel 7 to 40) corresponding to the blackbody portion of the spectrum, and the third is hard energy (pha channel 70 to 240) corresponding to the thermal brehmsstrahlung portion of the spectrum.

Table1 – Time Distribution of Observations

OBI	Time Start	Time Stop	Duration(sec)
1	9-MAR-91 21:38:29	9-MAR-91 22:10:28	1405
2	10-MAR-91 21:36:49	10-MAR-91 22:08:28	1302
3	10-MAR-91 23:11:59	10-MAR-91 23:39:58	882
4	11-MAR-91 21:36:48	11-MAR-91 22:04:28	1062
5	12-MAR-91 00:54:51	12-MAR-91 01:16:28	941
6	12-MAR-91 12:16:54	12-MAR-91 12:36:13	1107
7	12-MAR-91 20:05:53	12-MAR-91 20:33:13	1540
8	13-MAR-91 00:52:53	13-MAR-91 01:16:13	999
9	13-MAR-91 20:03:38	13-MAR-91 20:31:58	1480
10	14-MAR-91 00:52:42	14-MAR-91 01:15:43	1076
11	14-MAR-91 02:21:58	14-MAR-91 02:57:43	2075
12	14-MAR-91 10:40:24	14-MAR-91 10:59:53	1092
13	14-MAR-91 13:30:57	14-MAR-91 14:11:53	2299
14	14-MAR-91 15:10:08	14-MAR-91 15:47:27	2176

OBI 1 OBI 2

Total light curve

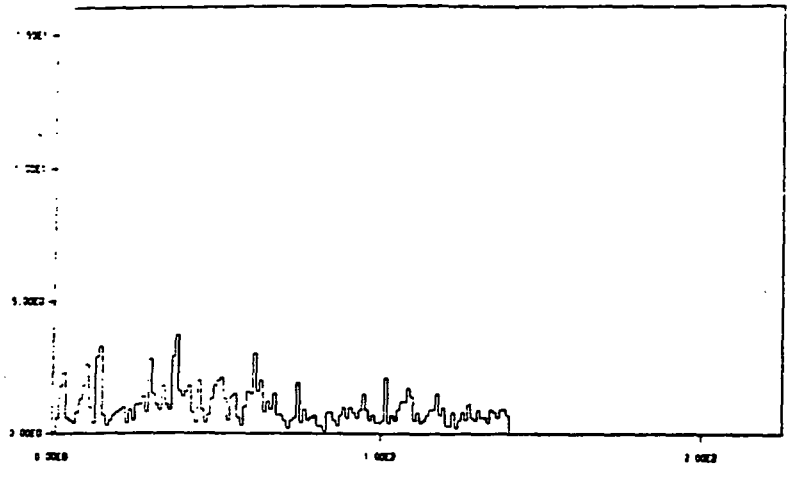

seconds (x10)

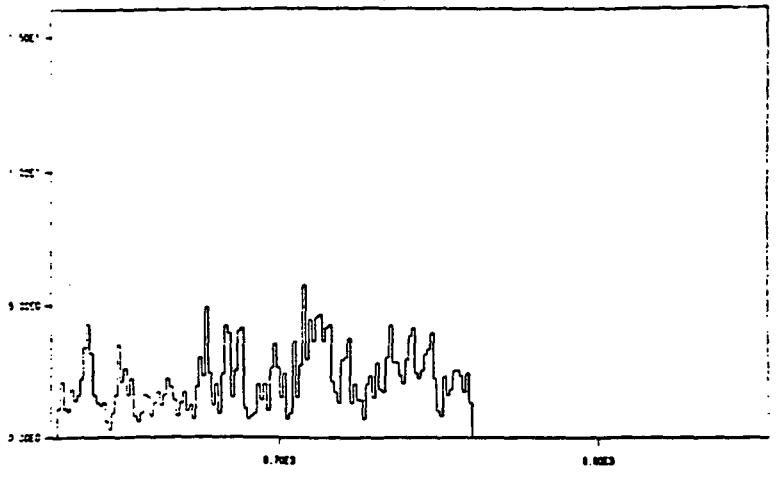

seconds(x10)

Soft Energy (PHA 7 to 40)

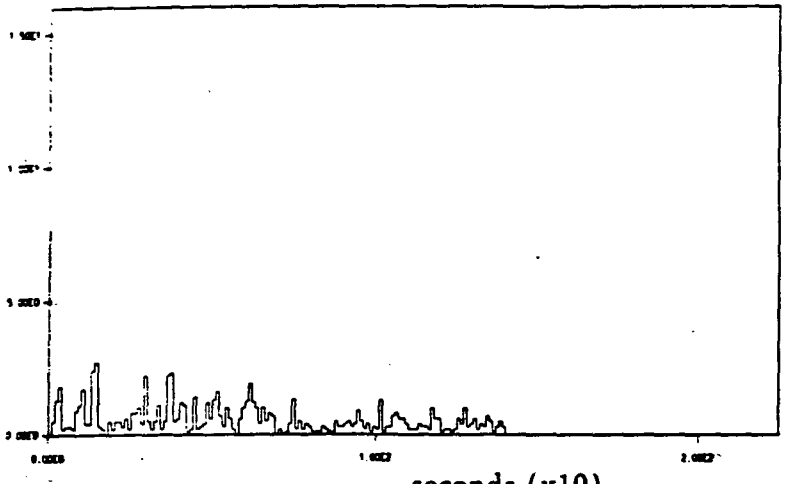

seconds (x10)

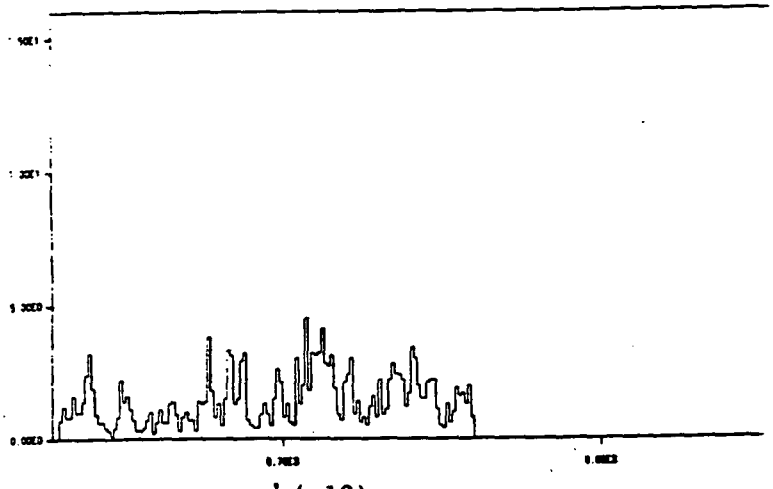

seconds(x10)

Hard Energy (PHA 70 to 240)

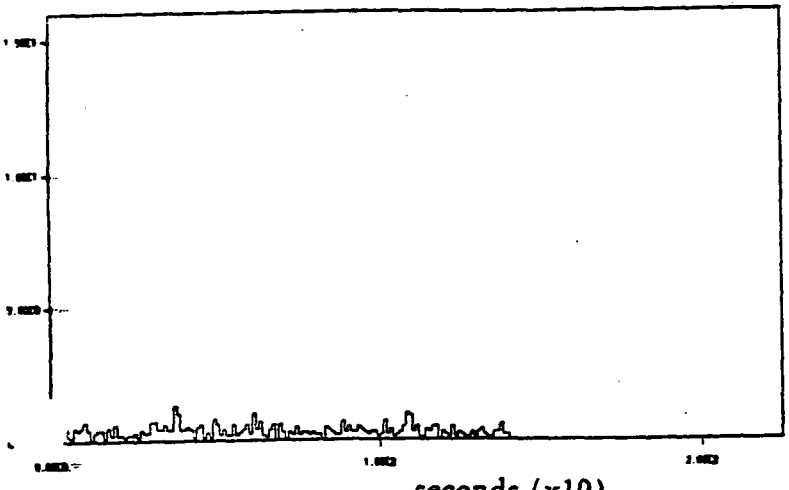

seconds (x10)

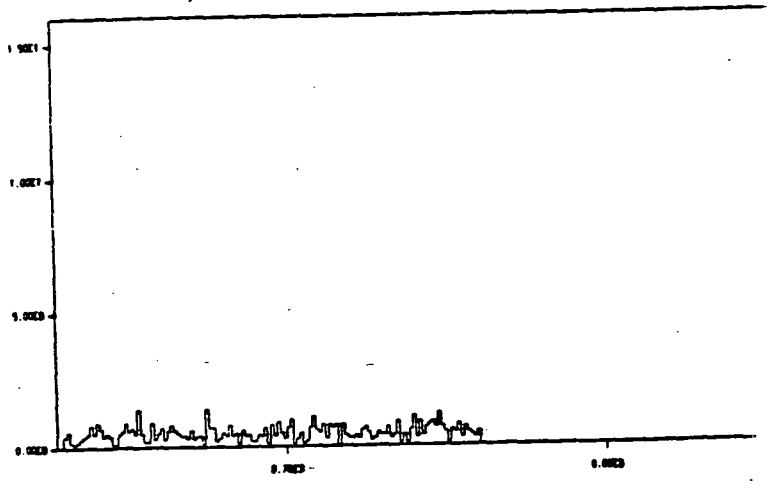

seconds(x10)

OBI 3 OBI 4

Total light curve

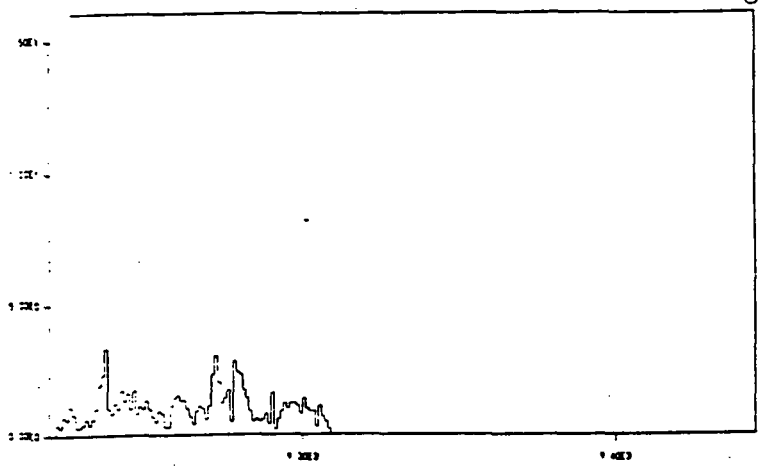

seconds (x10)

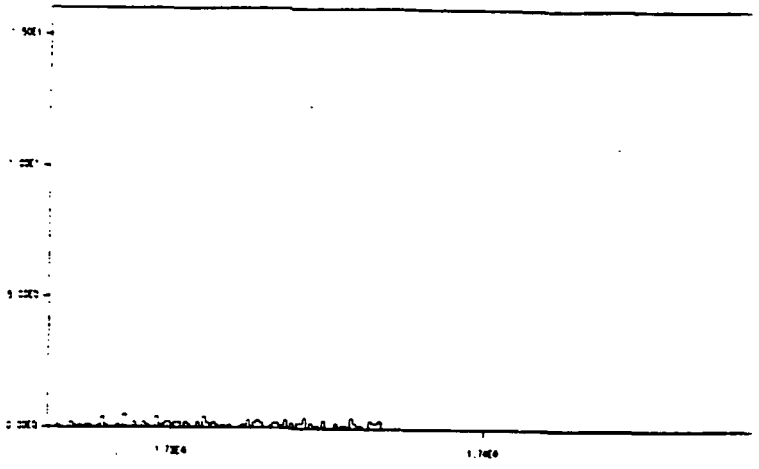

seconds(x10)

Soft Energy (PHA 7 to 40)

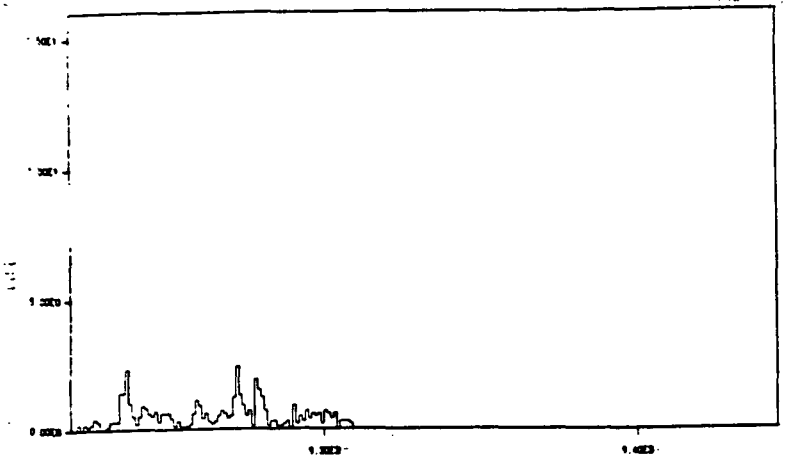

seconds (x10)

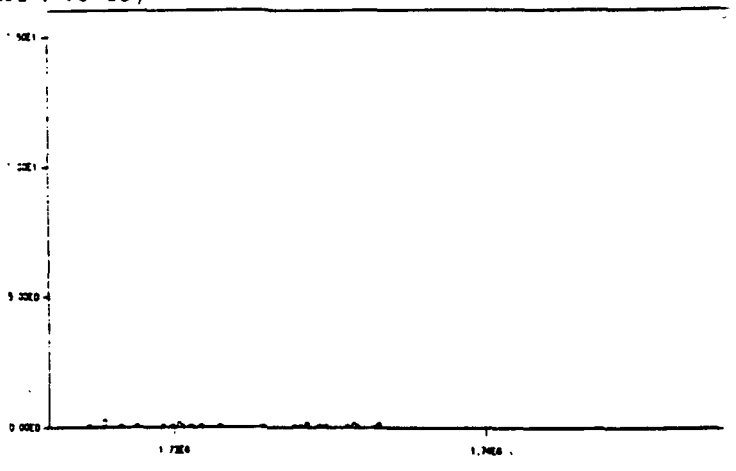

seconds(x10)

Hard Energy (PHA 70 to 240)

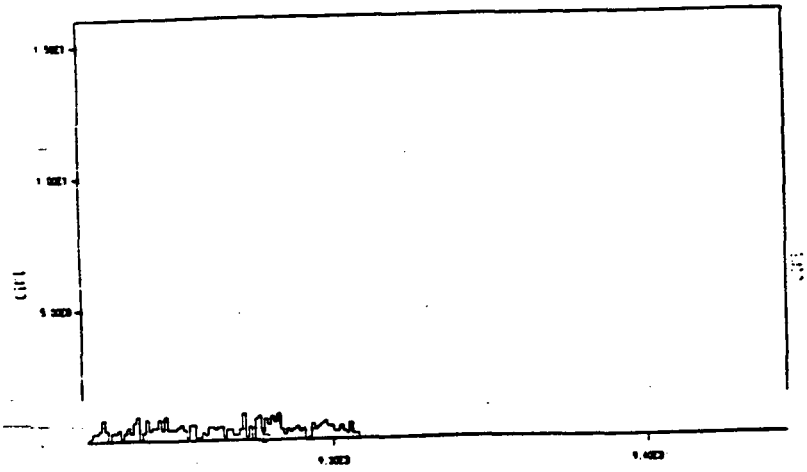

seconds (x10)

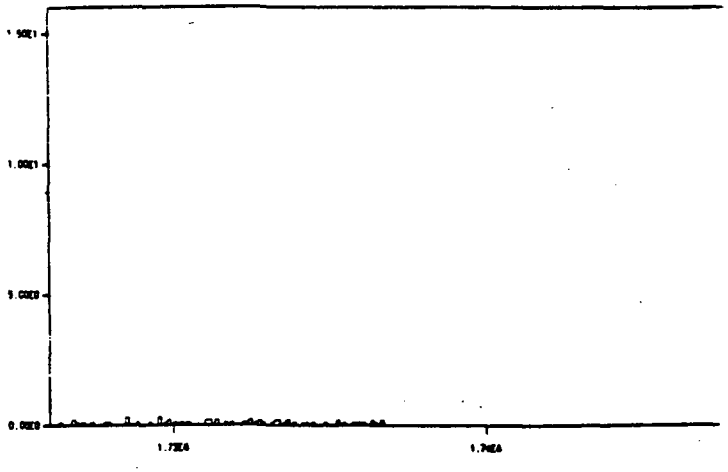

seconds(x10)

OBI 5 OBI 6

Total light curve

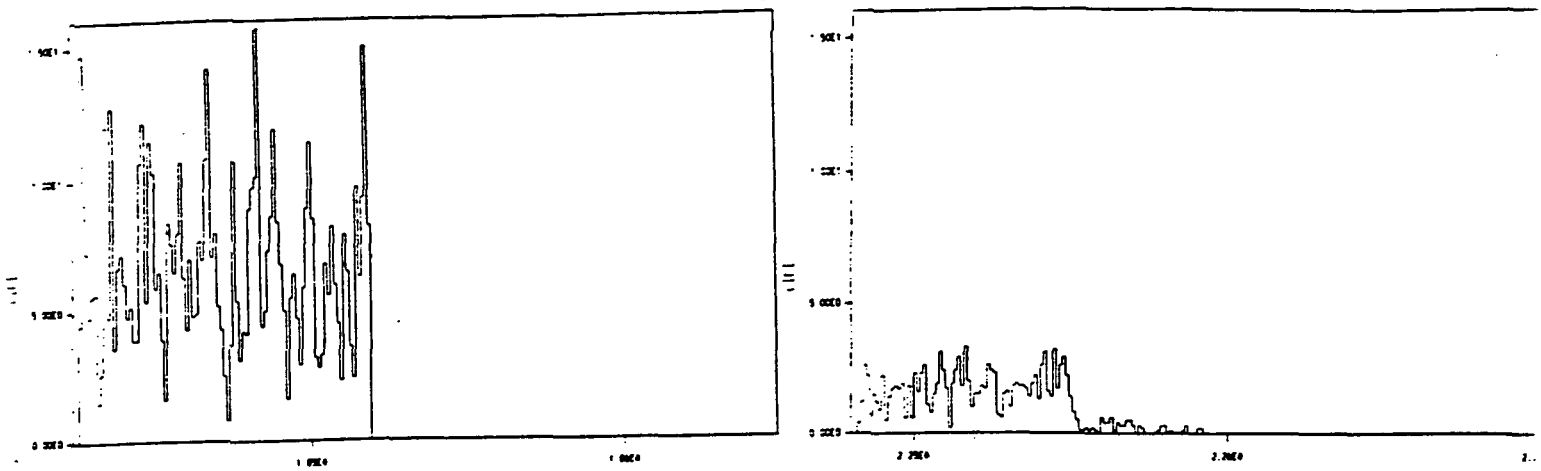

seconds (x10) seconds(x10)

Soft Energy (PHA 7 to 40)

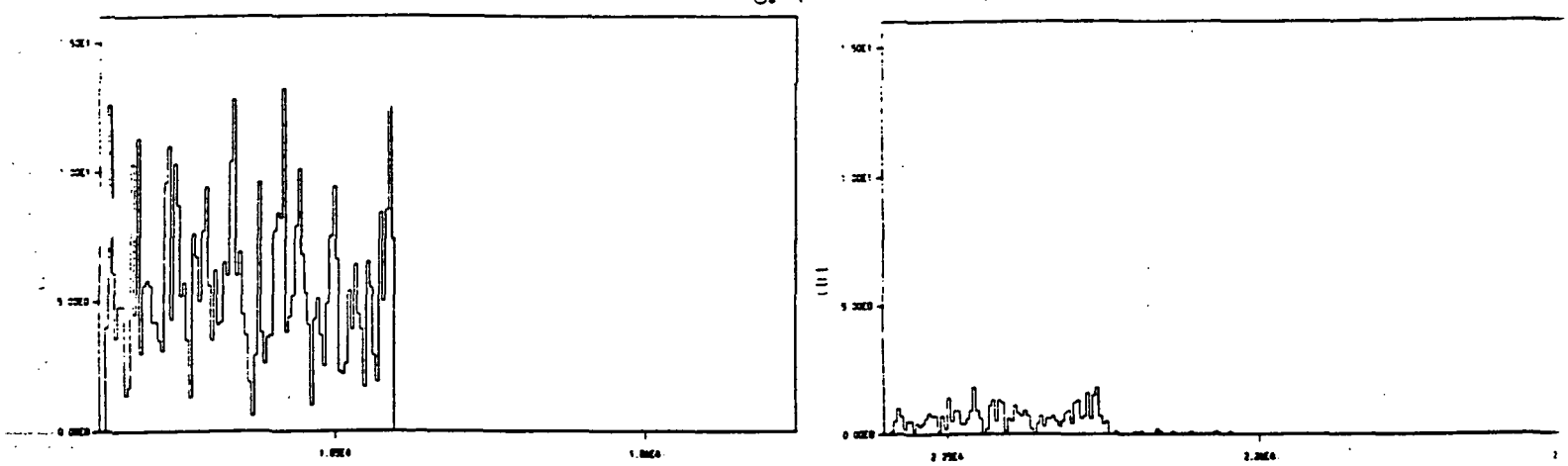

seconds (x10) seconds(x10)

Hard Energy (PHA 70 to 240)

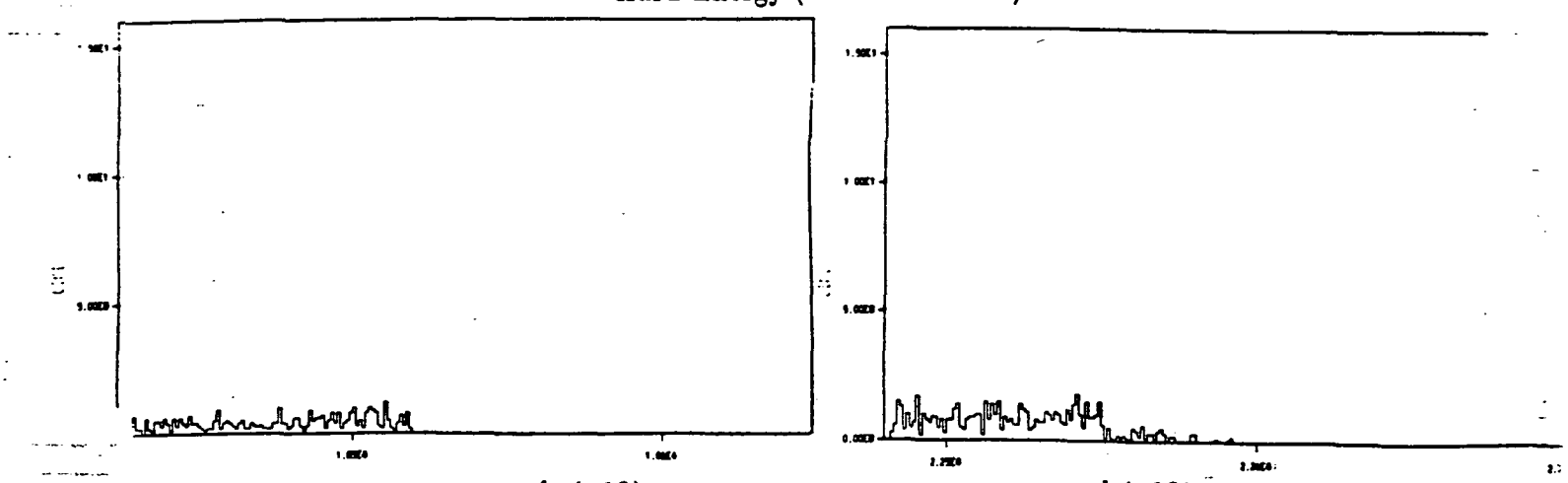

seconds (x10) seconds(x10)

OBI 7 OBI 8

Total light curve

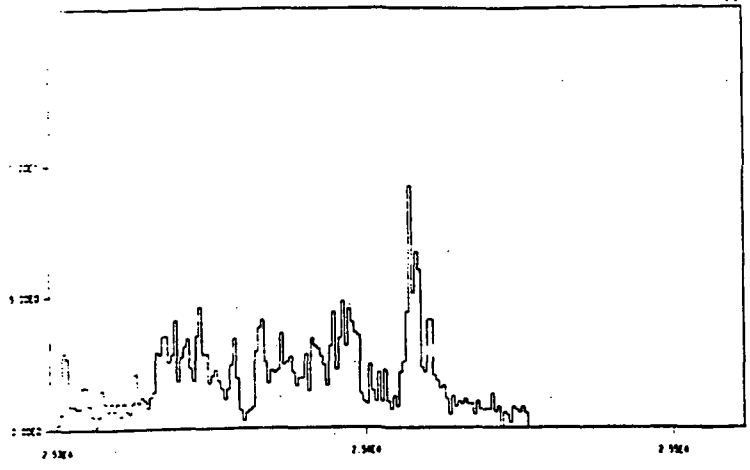

seconds (x10)

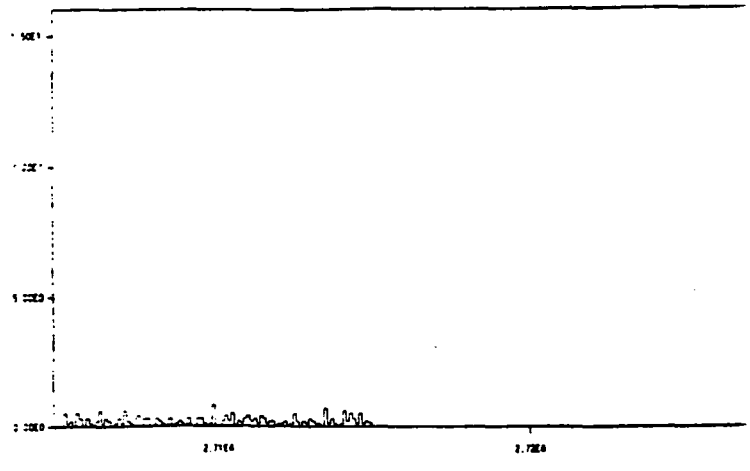

seconds(x10)

Soft Energy (PHA 7 to 40)

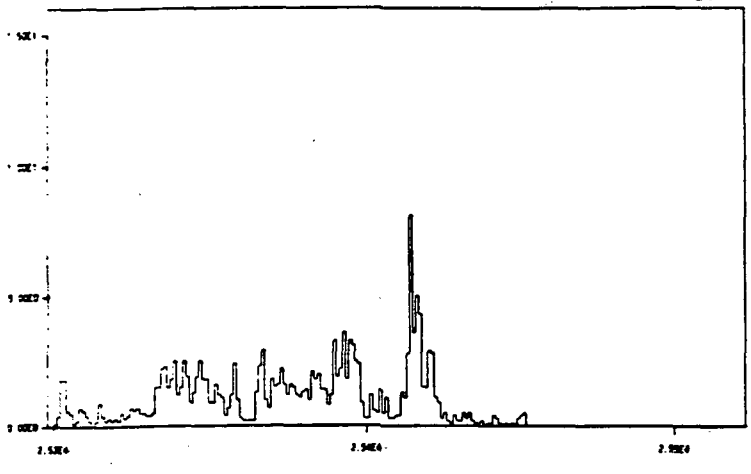

seconds (x10)

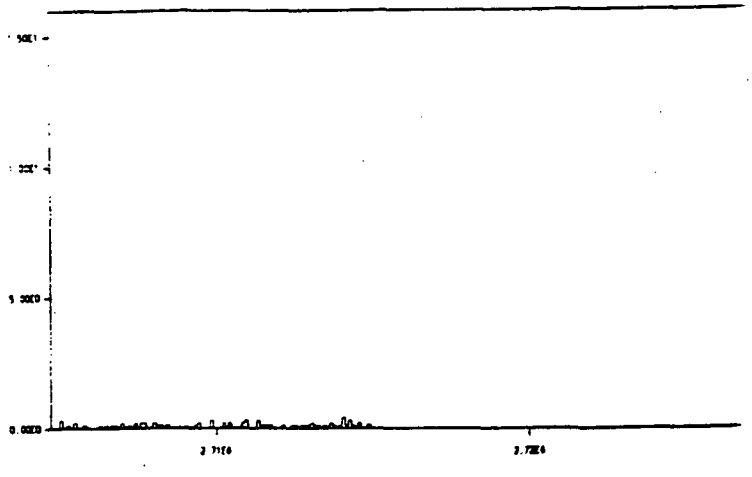

seconds(x10)

Hard Energy (PHA 70 to 240)

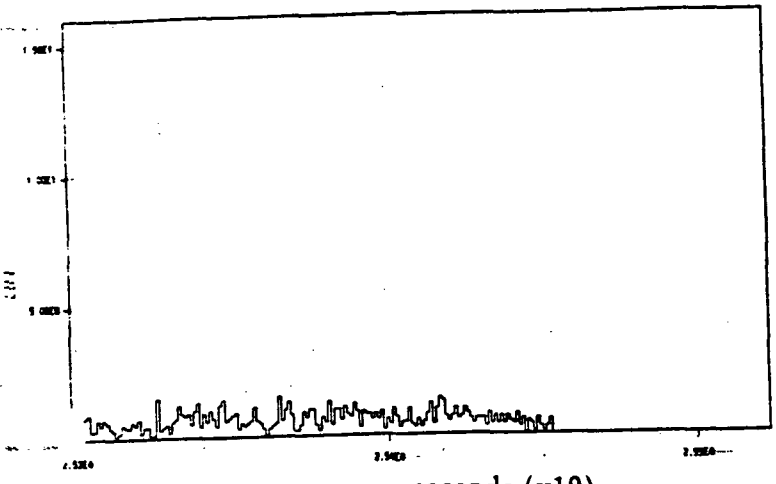

seconds (x10)

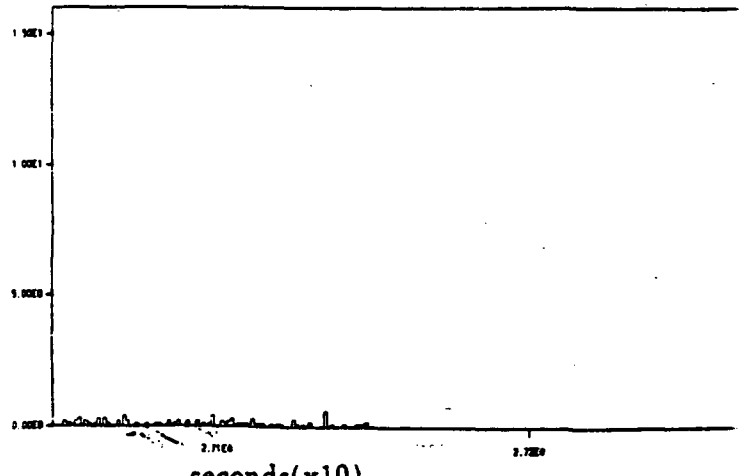

seconds(x10)

OBI 9 OBI 10

Total light curve

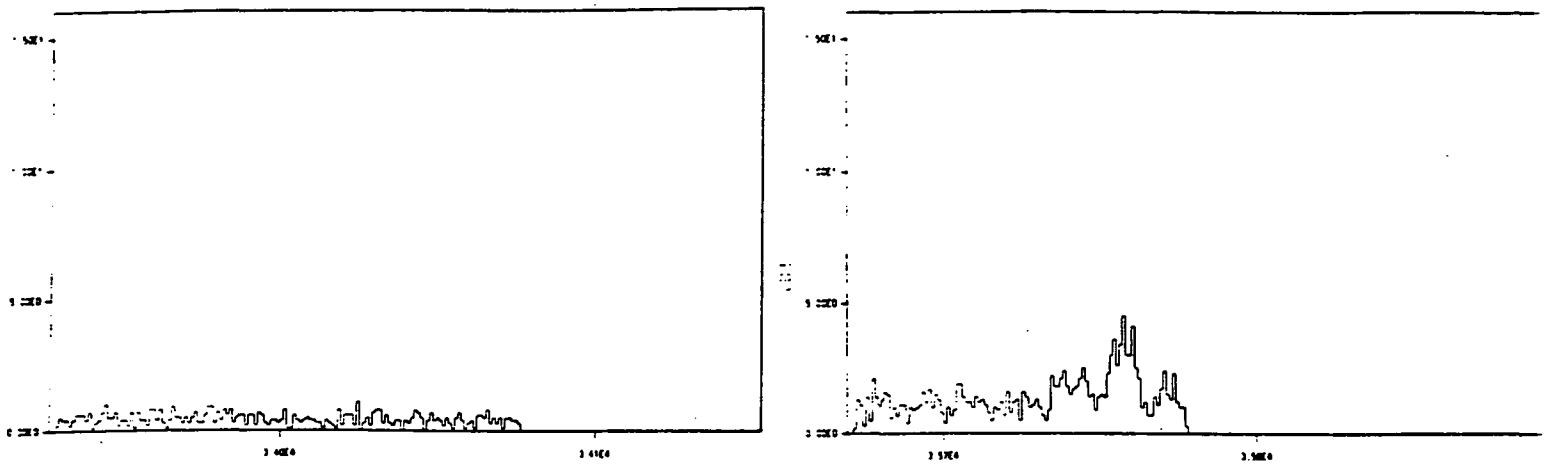

seconds (x10) seconds(x10)

Soft Energy (PHA 7 to 40)

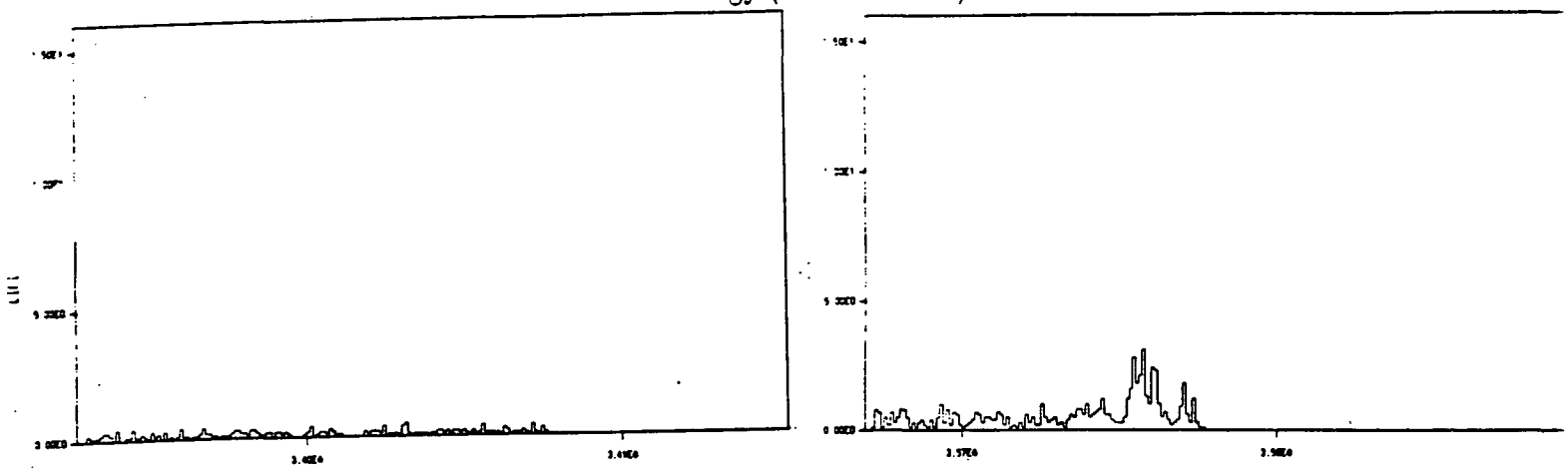

seconds (x10) seconds(x10)

Hard Energy (PHA 70 to 240)

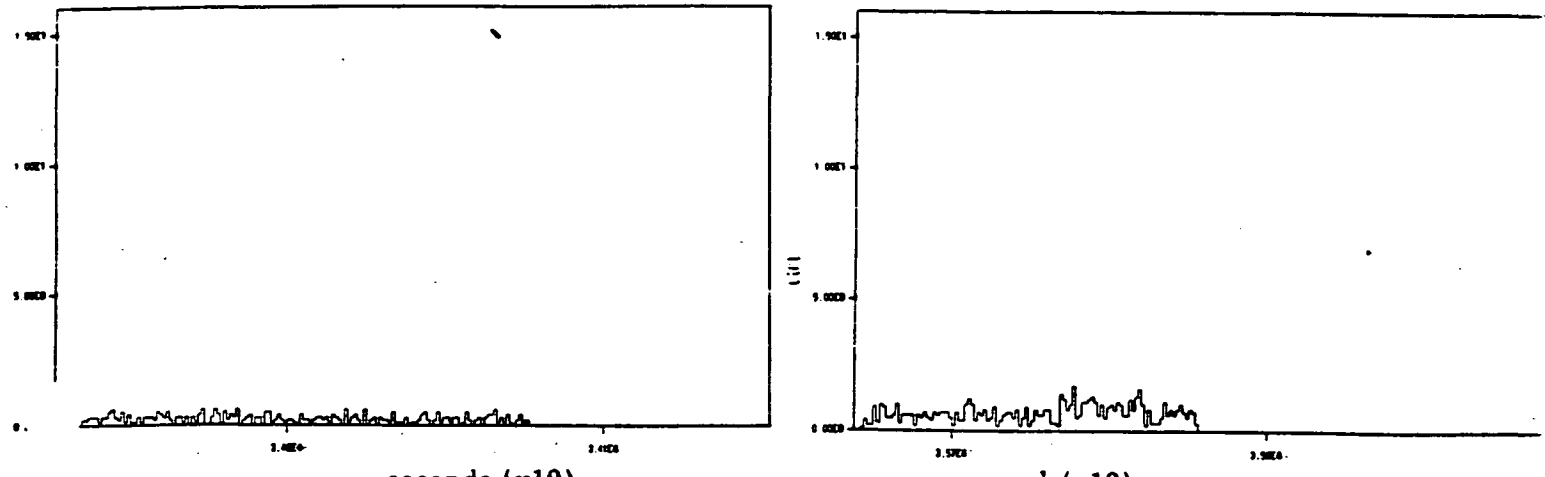

seconds (x10) seconds(x10)

OBI 11 OBI 12

Total light curve

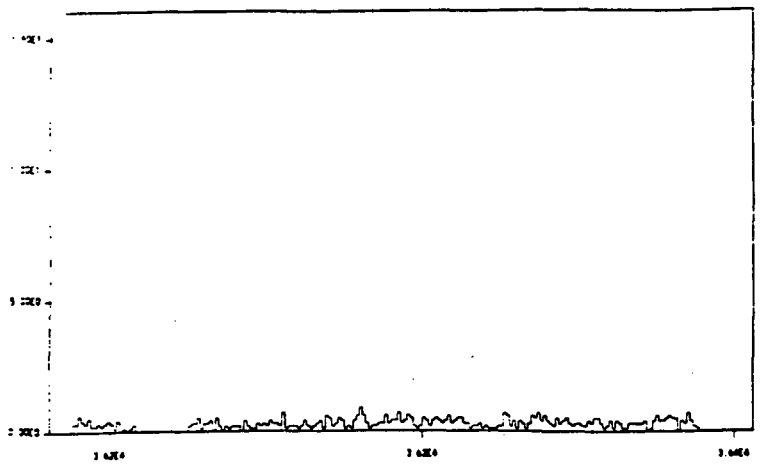

seconds (x10)

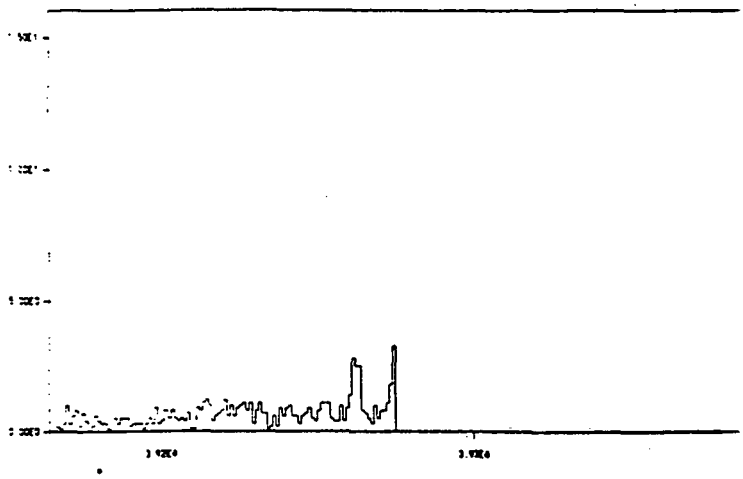

seconds(x10)

Soft Energy (PHA 7 to 40)

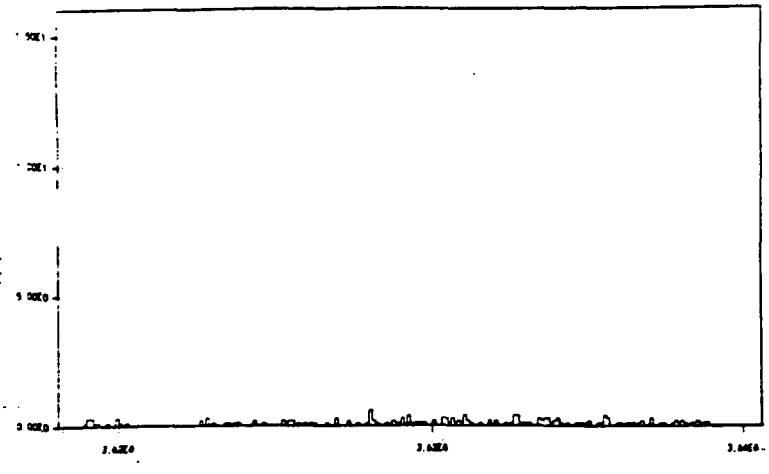

seconds (x10)

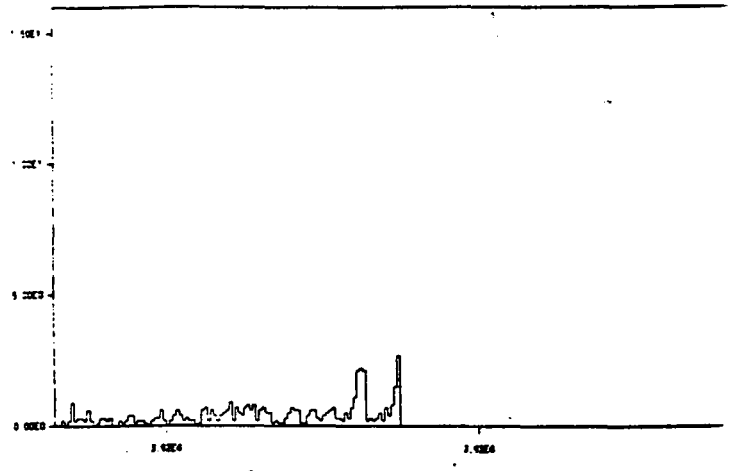

seconds(x10)

Hard Energy (PHA 70 to 240)

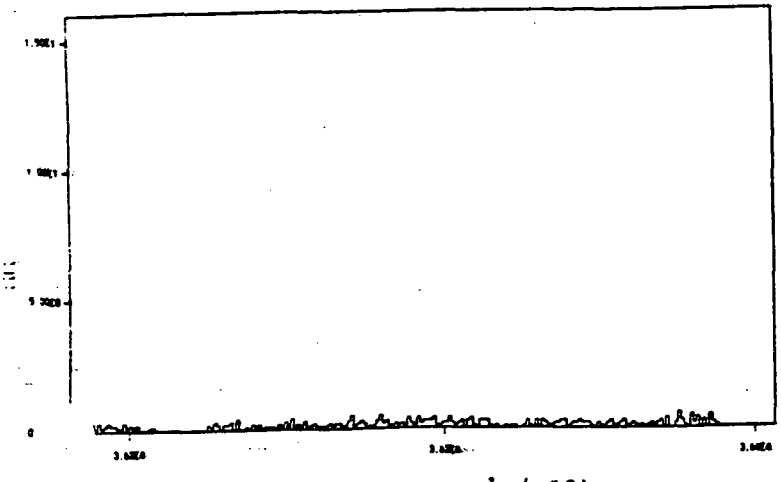

seconds (x10)

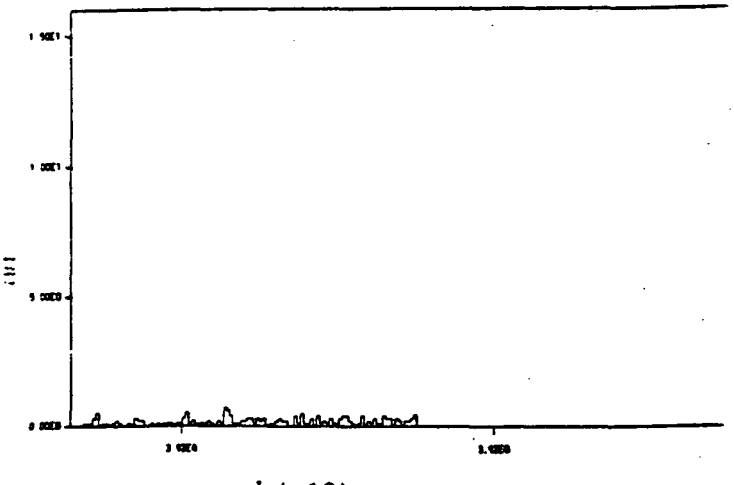

seconds(x10)

OBI 13 OBI 14

Total light curve

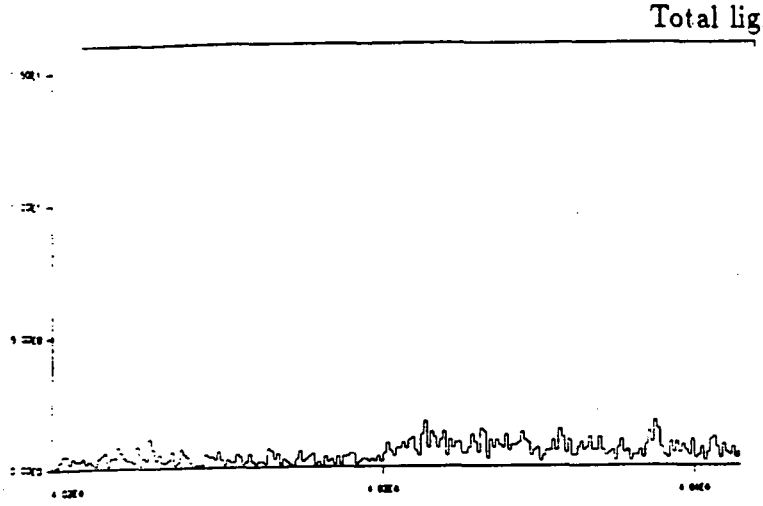

seconds (x10)

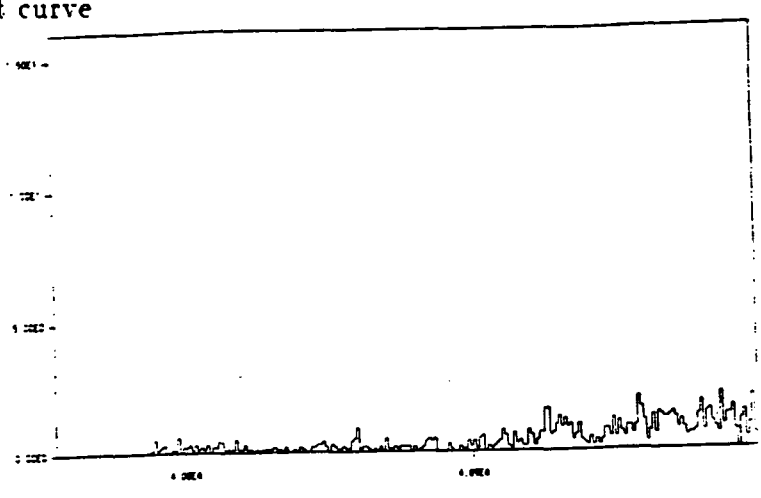

seconds(x10)

Soft Energy (PHA 7 to 40)

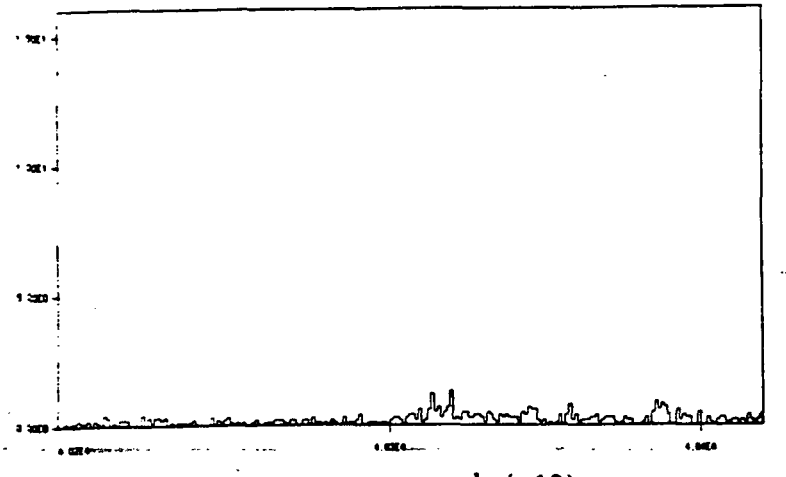

seconds (x10)

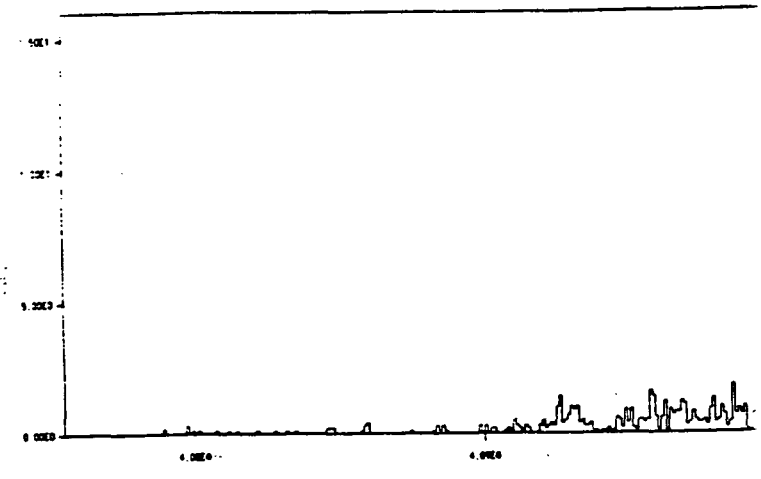

seconds(x10)

Hard Energy (PHA 70 to 240)

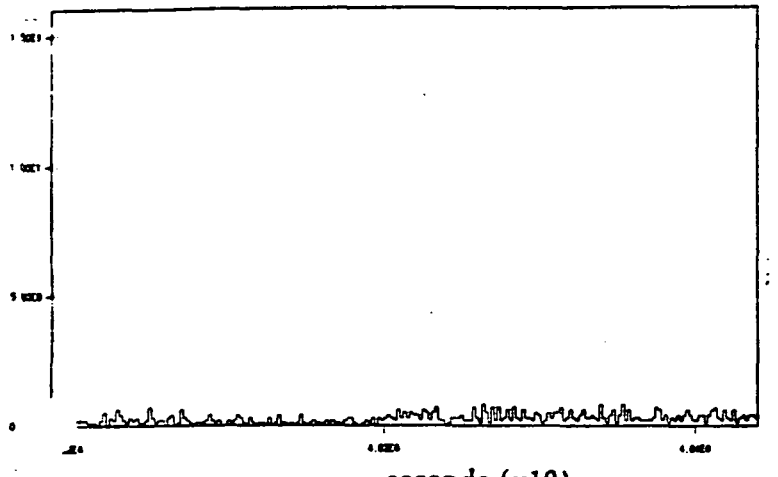

seconds (x10)

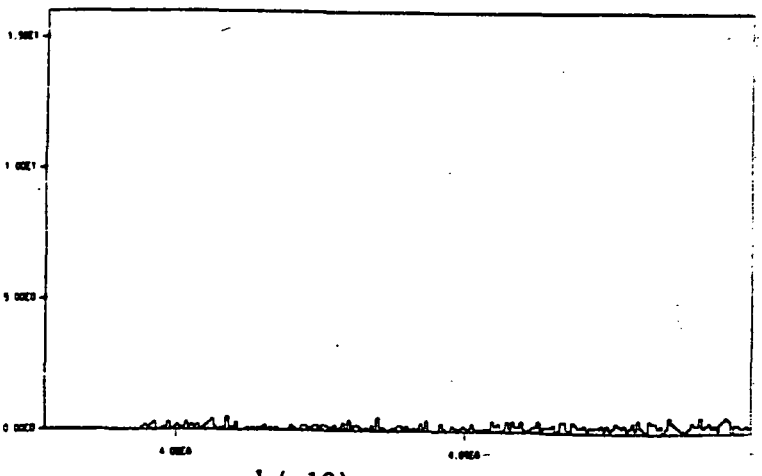

seconds(x10)

Appendix B

Spectra

The following pages contain plots of the spectra for each of the individual intervals, plotted with the best fit, as found using the PROS Simplex fit routine.

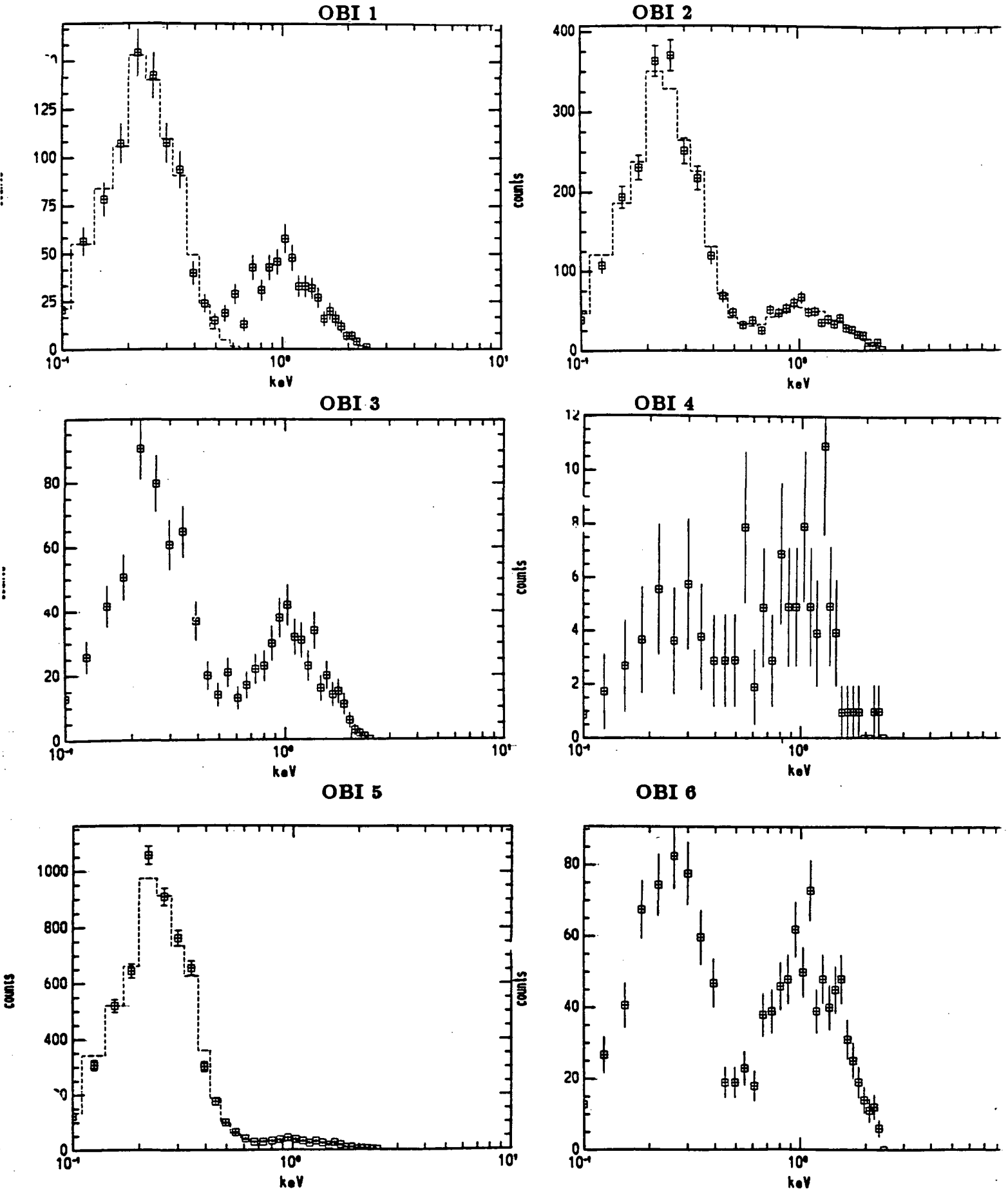
OBI 1
OBI 2
OBI 3
OBI 4
OBI 5
OBI 6
counts
keV

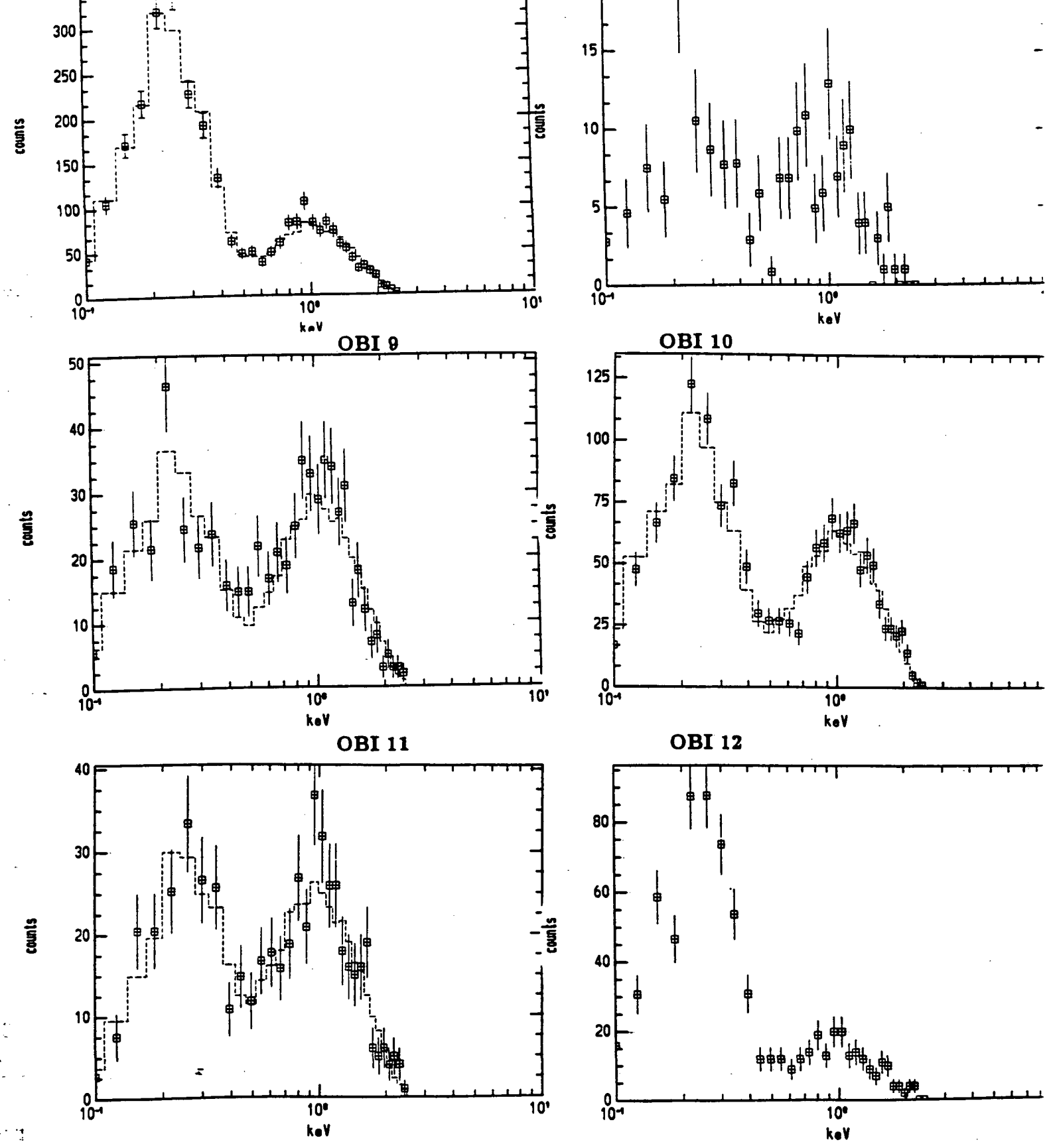
OBI 7
OBI 8
OBI 9
OBI 10
OBI 11
OBI 12
counts
keV

OBI 13

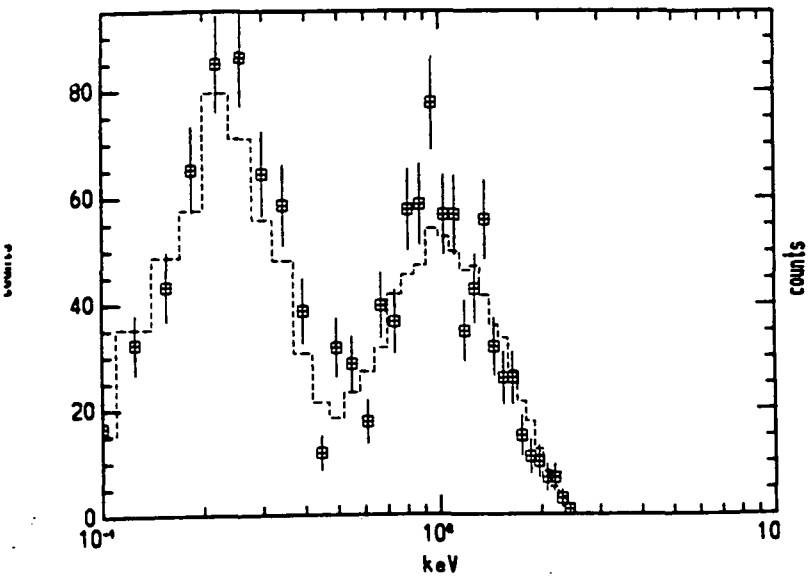

OBI 14

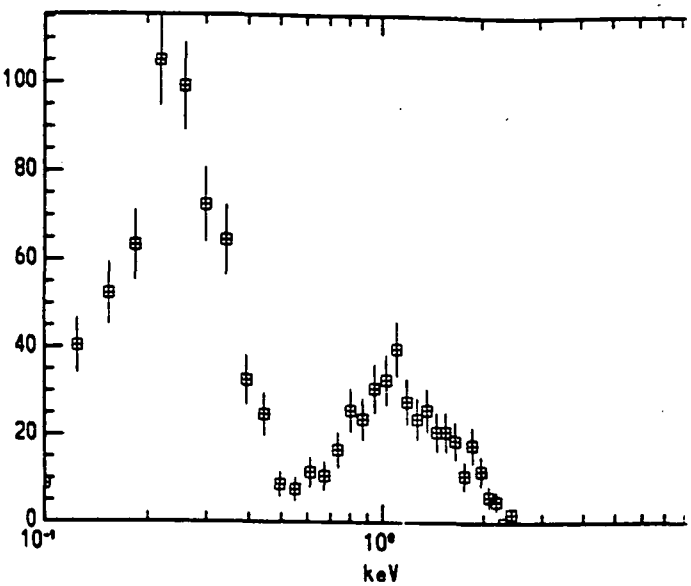

Total

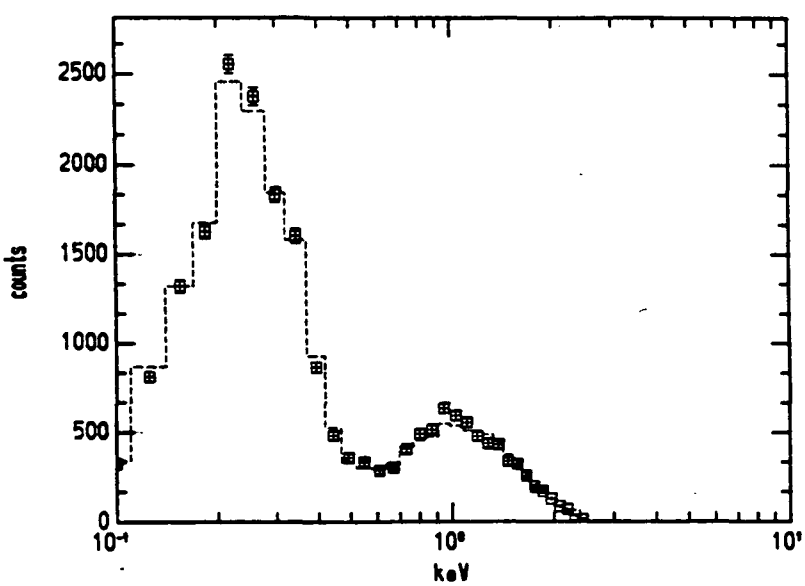

Appendix C

Cross Correlation

The following plots are of cross-correlations between the hard and soft energy bands for each OBI. There are also plots of their autocorrelations.

Cross - Correlations

OBI-1

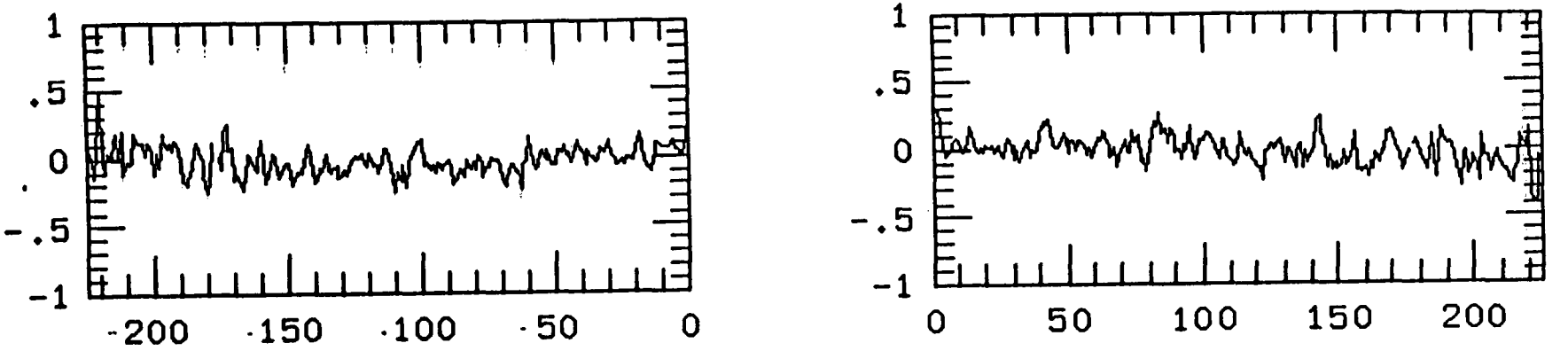

Phase shift (sec x 5.62)

OBI 2

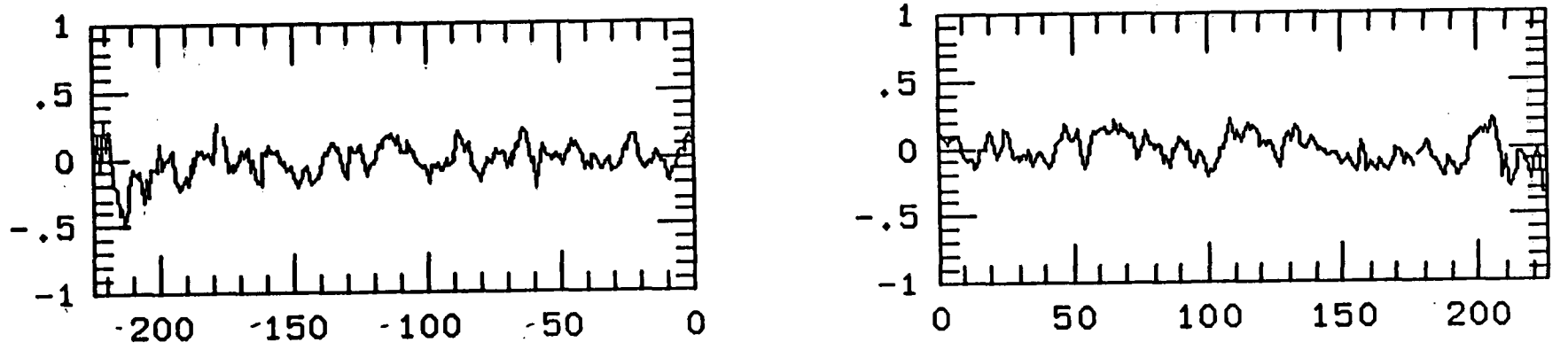

Phase Shift (sec x 5.21)

OBI-3

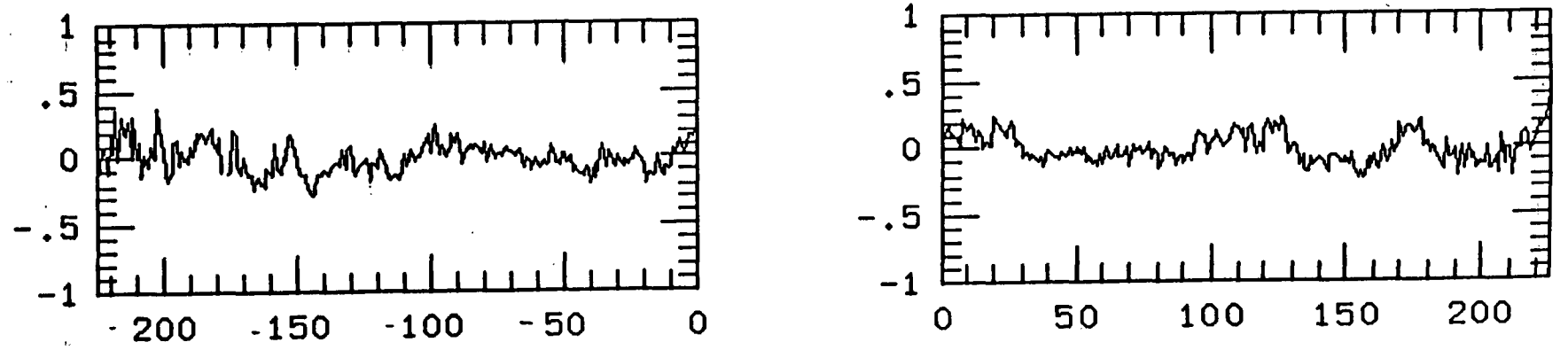

Phase Shift (x 3.53 = sec)

OBI 4

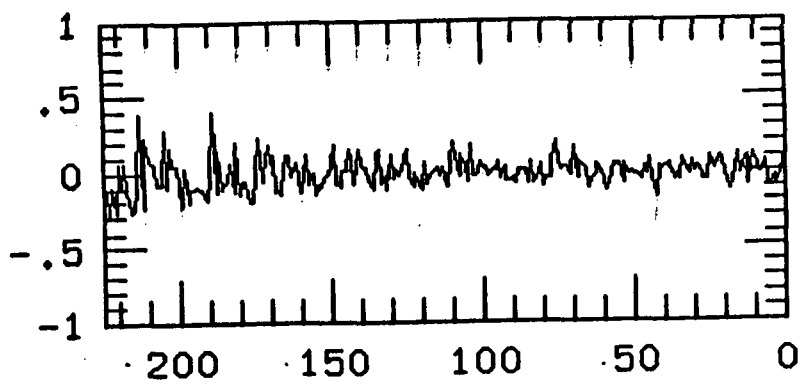

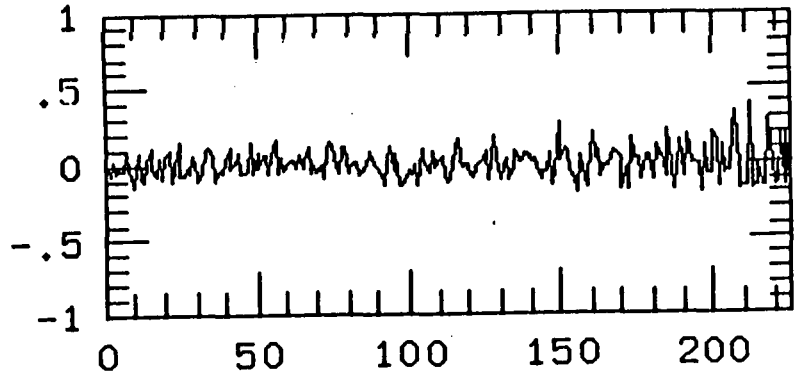

Phase Shift (x 4.25 = sec)

OBI 5

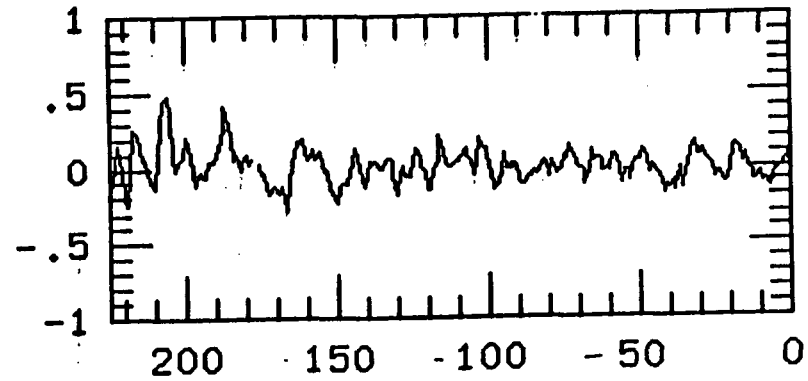

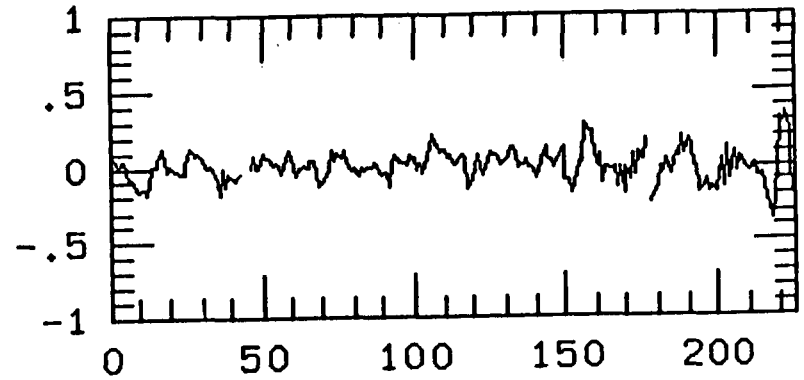

Phase Shift (x 3.76 = sec)

OBI 6

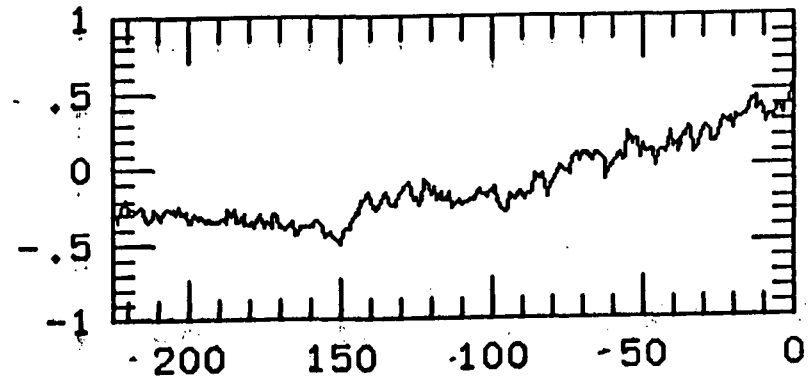

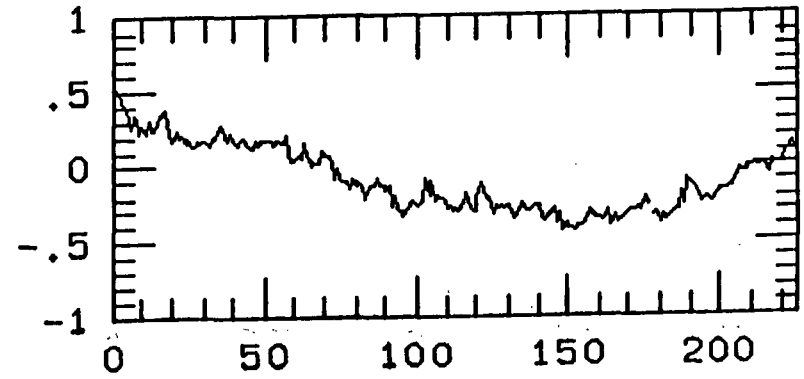

Phase Shift (x 4.43 = sec)

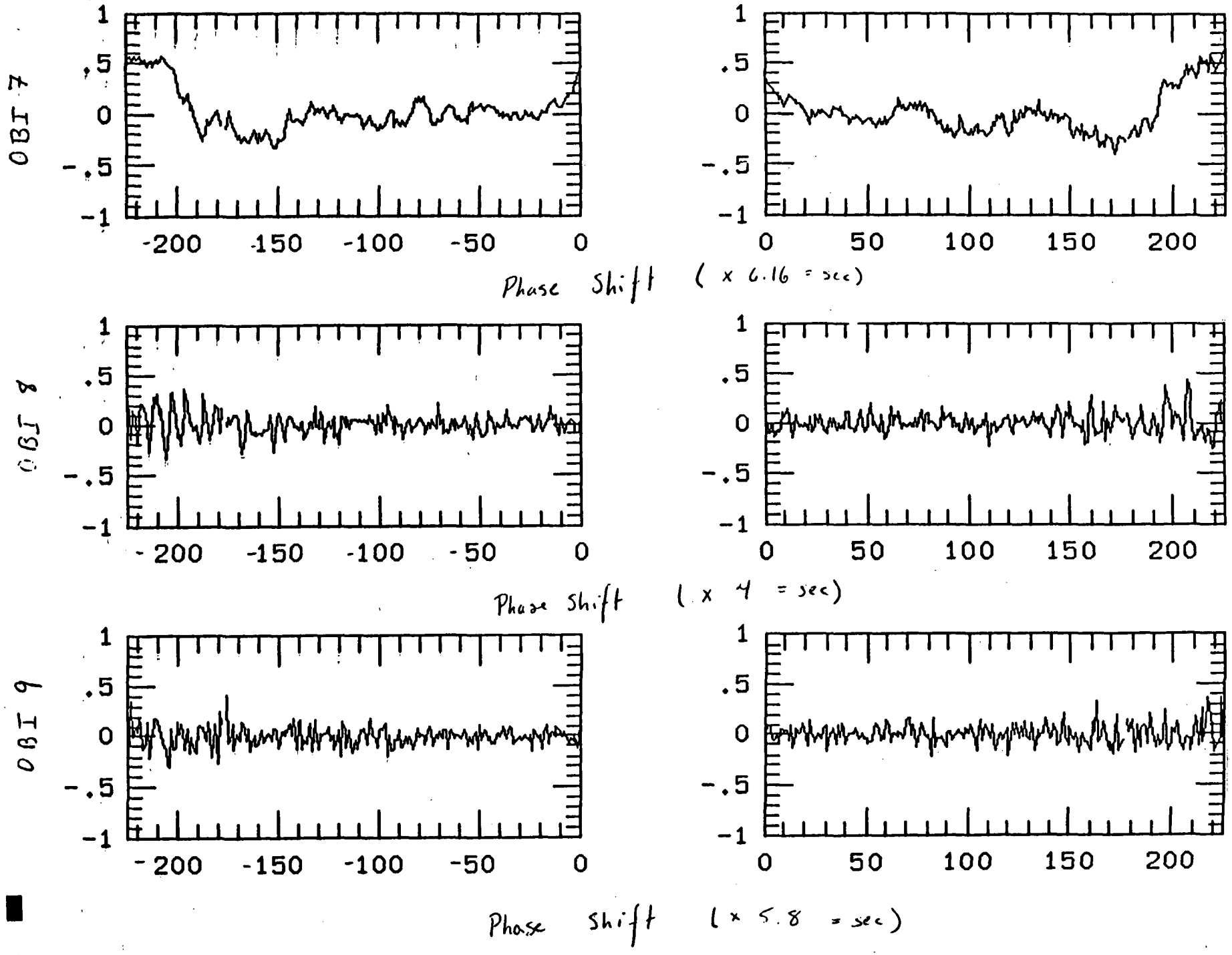
OBI 7
OBI 8
OBI 9
1
.5
0
-.5
-1
-200
-150
-100
-50
0
50
100
150
200
Phase Shift (x 6.16 = sec)
Phase Shift (x 4 = sec)
Phase Shift (x 5.8 = sec)

OBI 10

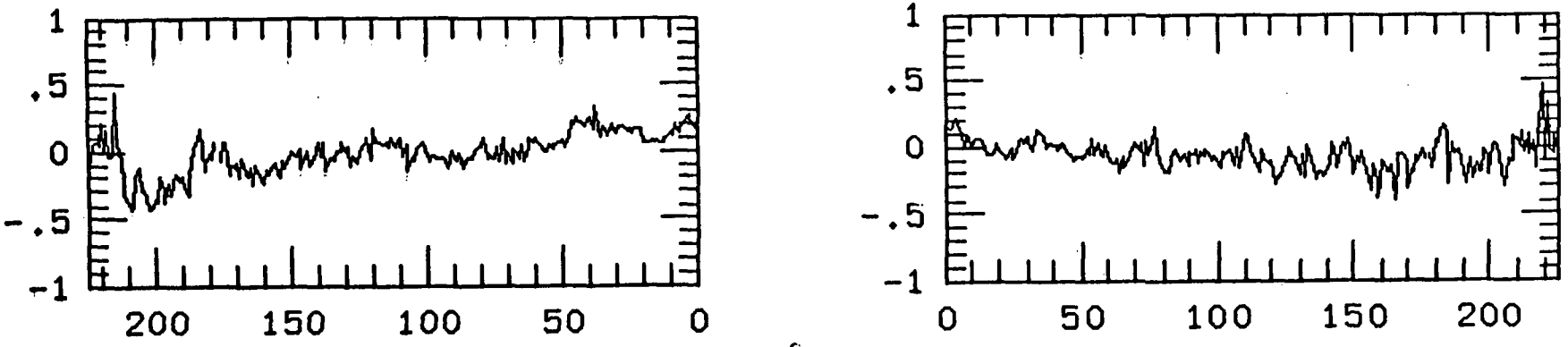

Phase shift (x 4.3 = sec)

OBI 11

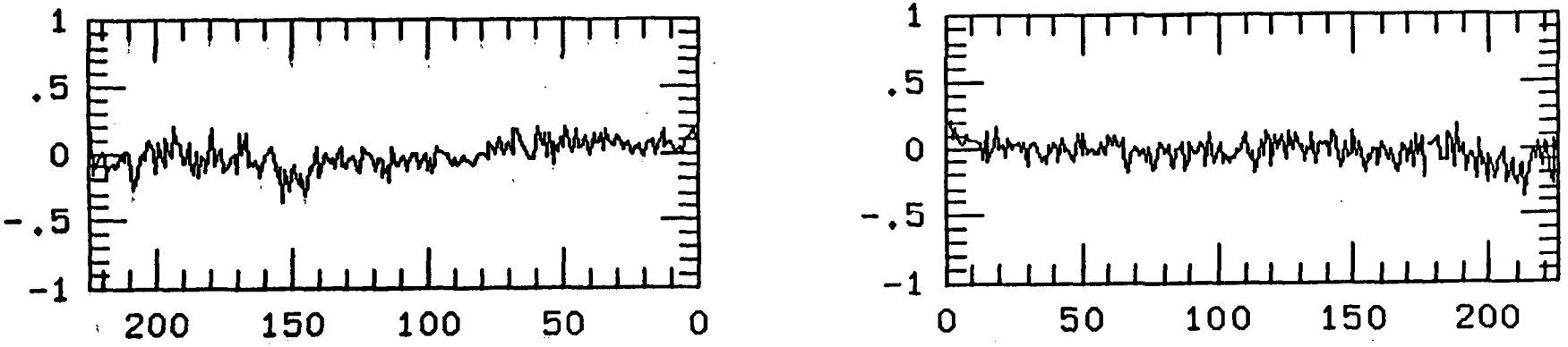

Phase shift (x 8.3 = sec)

OBI 12

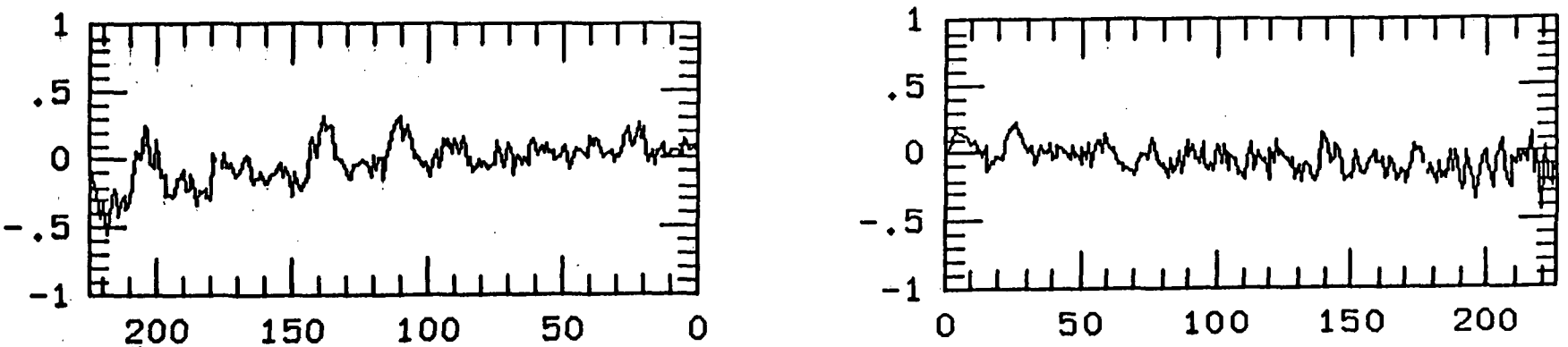

Phase shift (x 4.37 = sec)

OBI 13

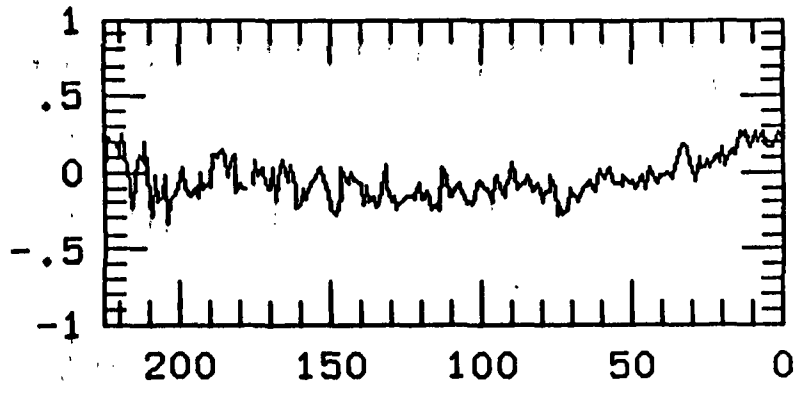

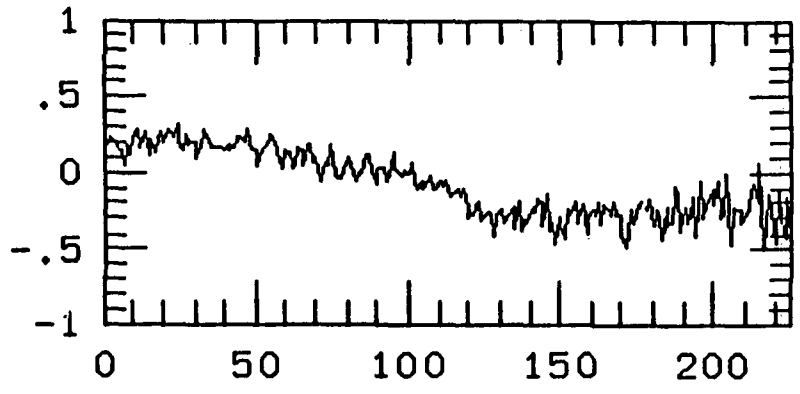

Phase shift (× 1.2 = sec)

OBI 14

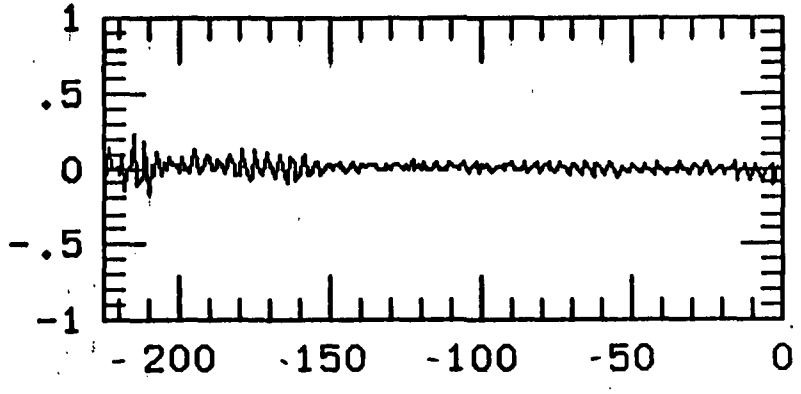

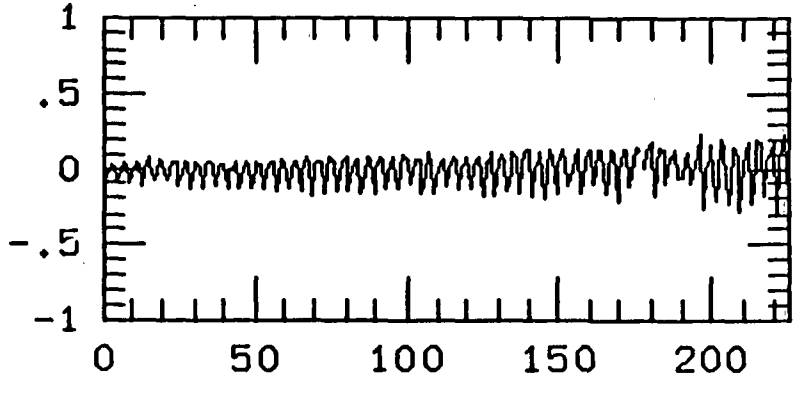

Phase shift (× 8.7 = sec)

Autocorrelations

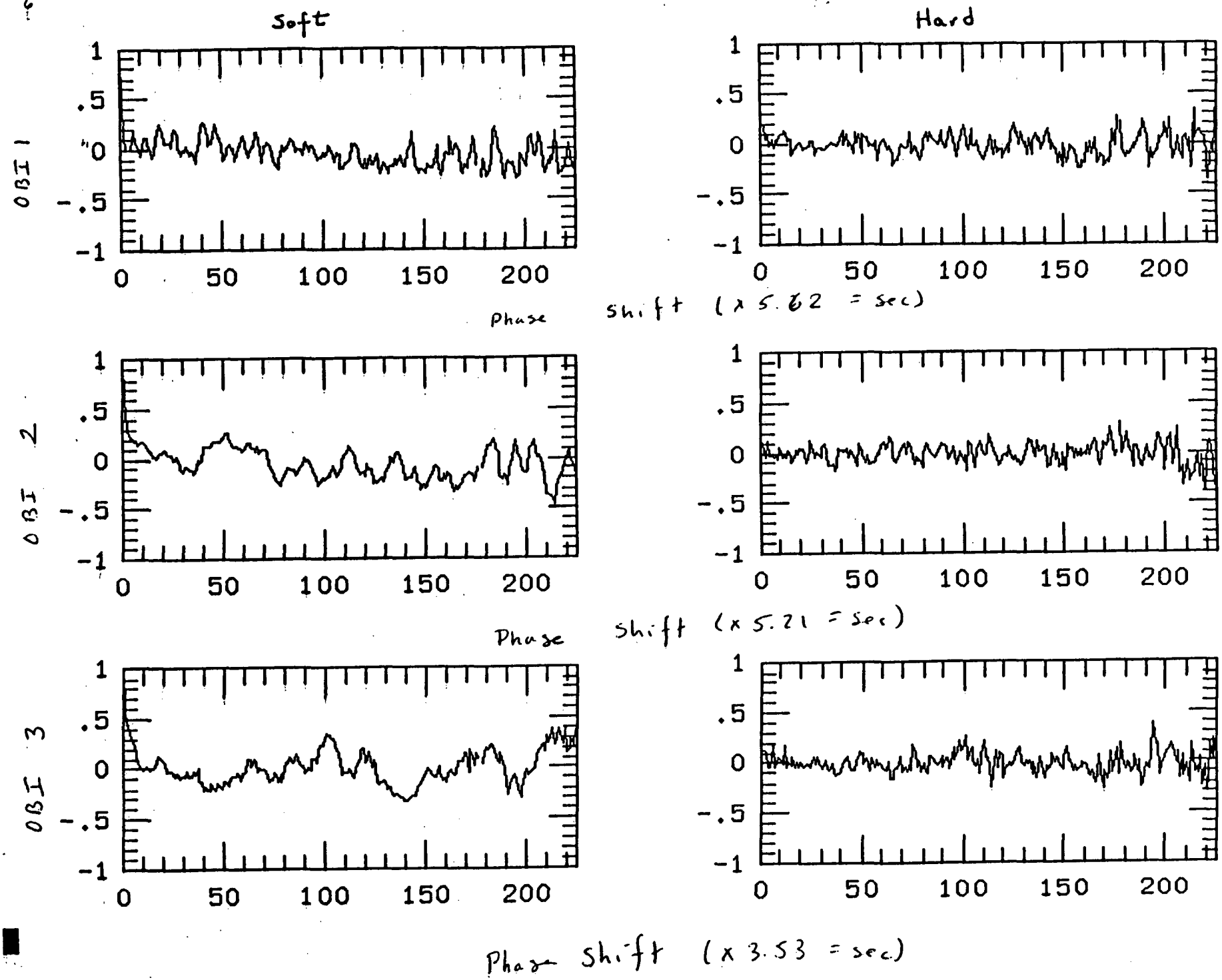

7

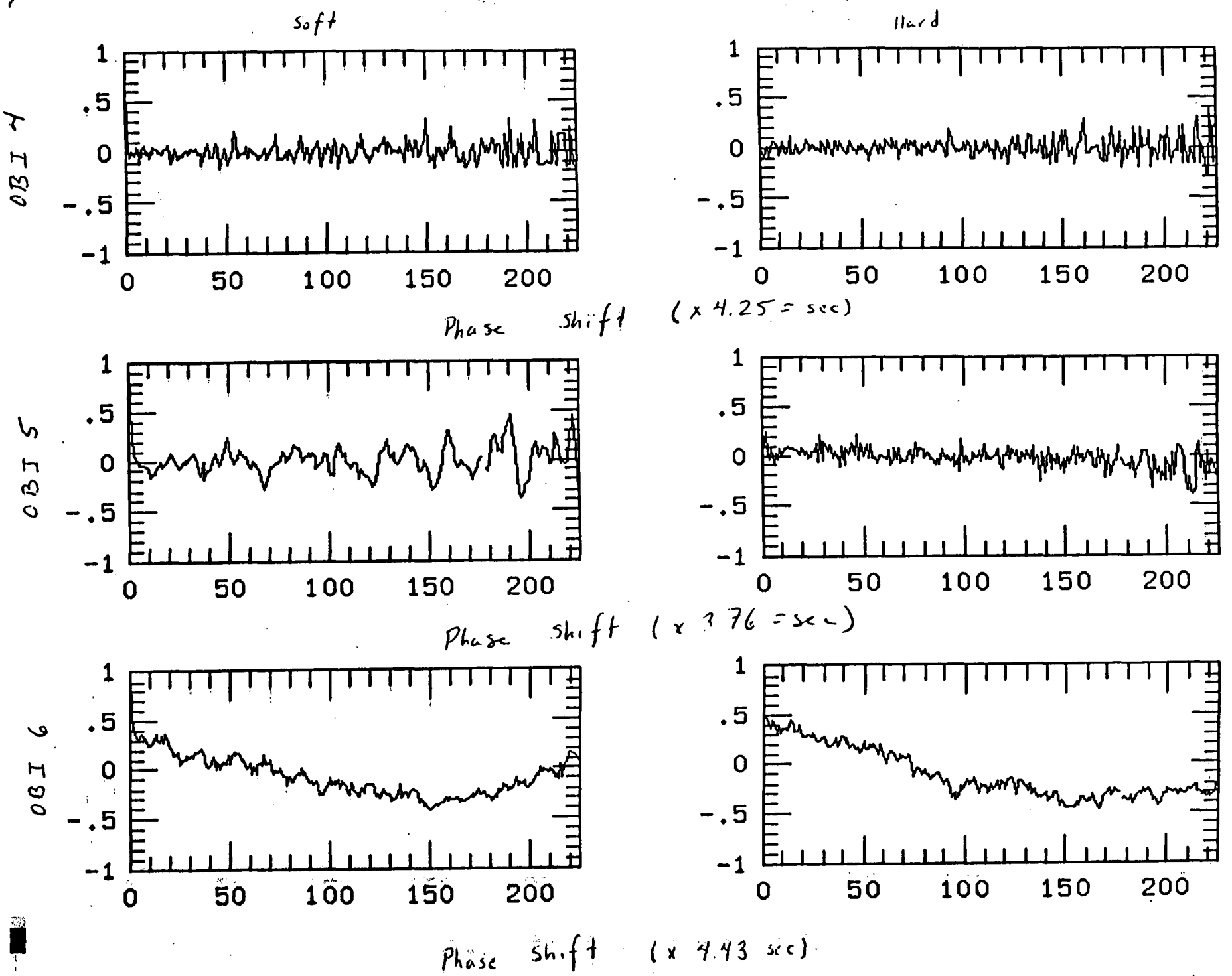
soft
hard
OBI 4
OBI 5
OBI 6
1
.5
0
-.5
-1
0
50
100
150
200
Phase shift (x 4.25 = sec)
Phase shift (x 3.76 = sec)
Phase shift (x 4.43 sec)

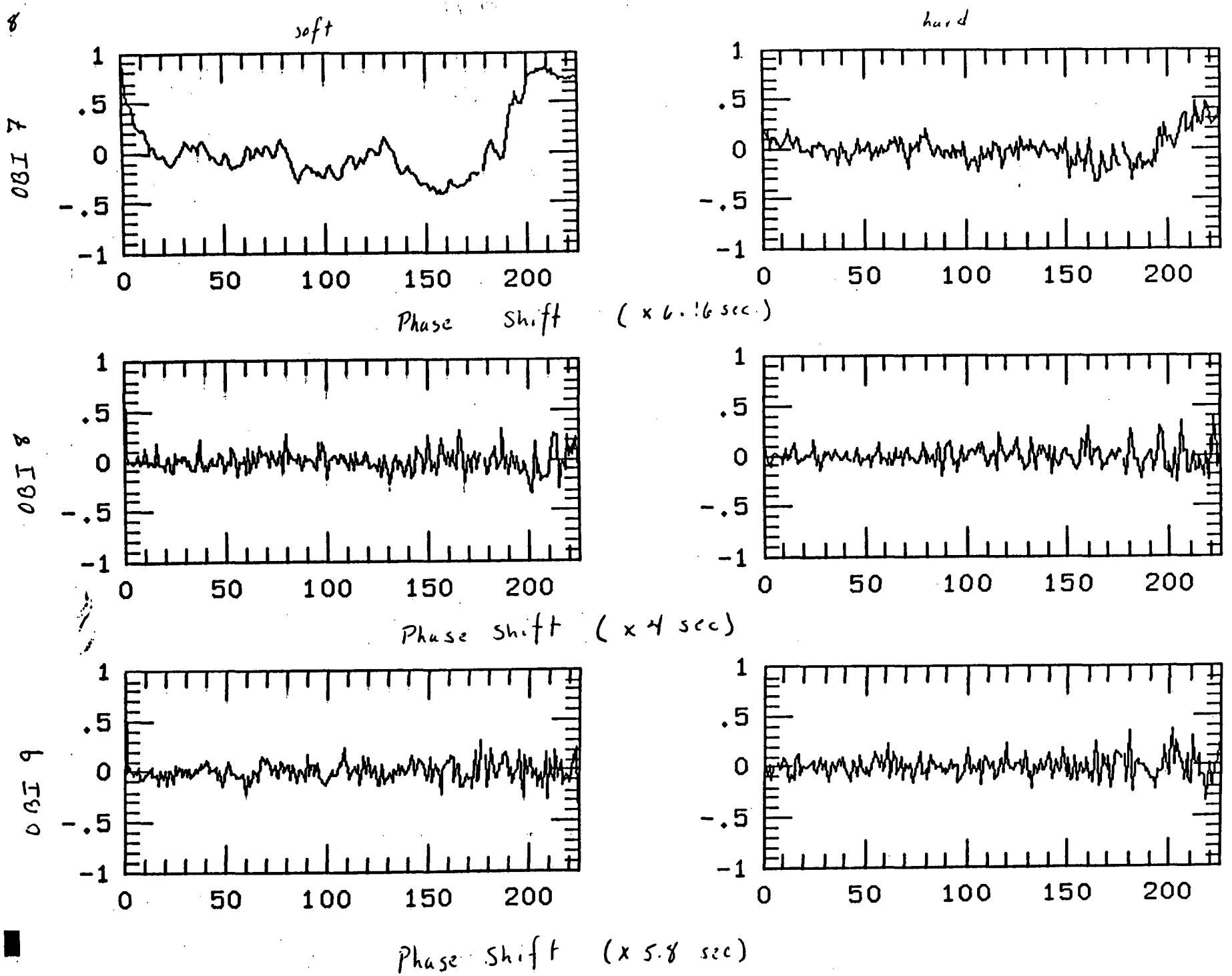
soft
hard
OBI 7
OBI 8
OBI 9
1
.5
0
-.5
-1
0
50
100
150
200
Phase Shift (x 6.16 sec)
Phase Shift (x 4 sec)
Phase Shift (x 5.8 sec)

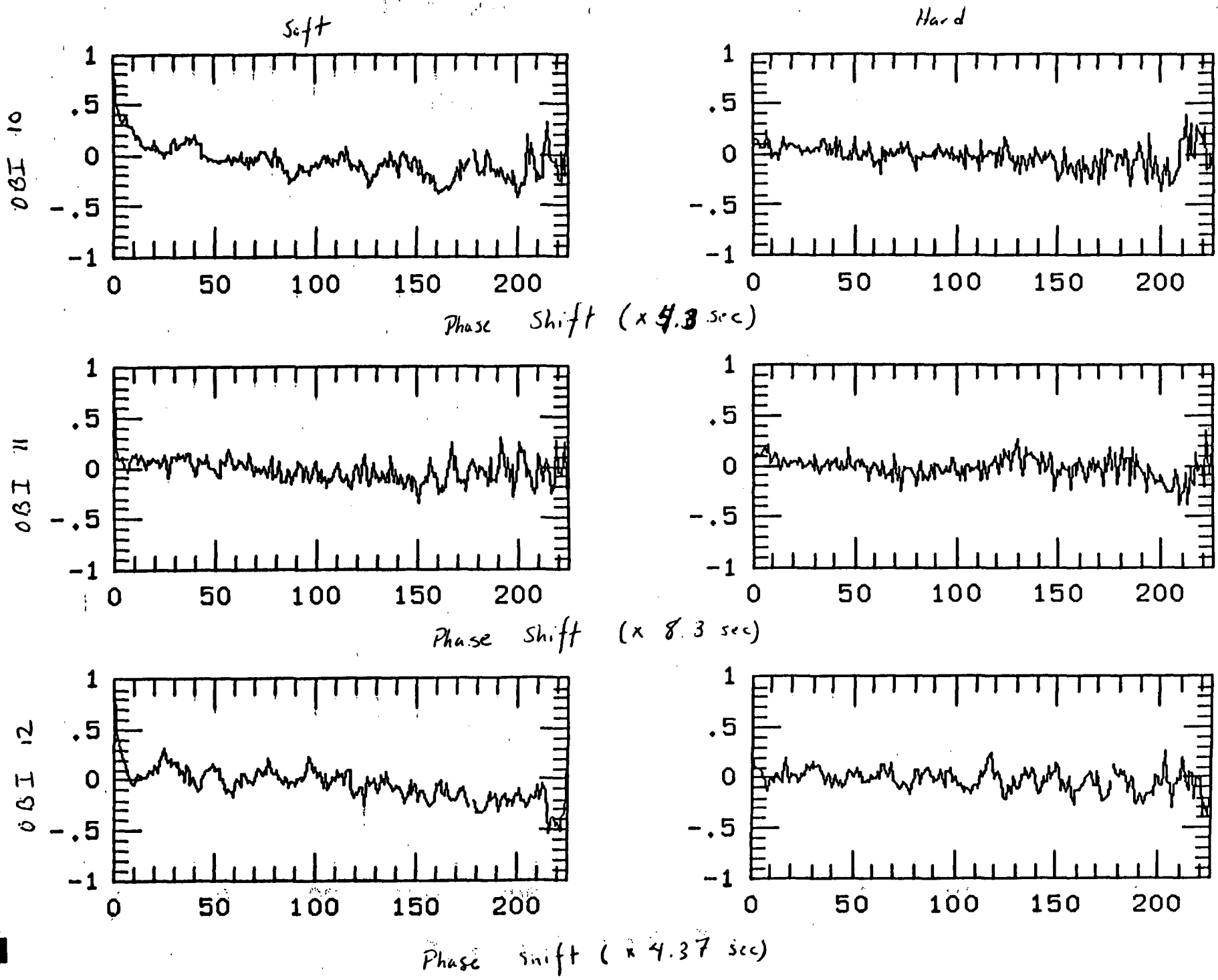
Soft
Hard
OBI 10
OBI 11
OBI 12
1
.5
0
-.5
-1
0
50
100
150
200
Phase Shift (x 4.3 sec)
Phase Shift (x 8.3 sec)
Phase Shift (x 4.37 sec)

Soft

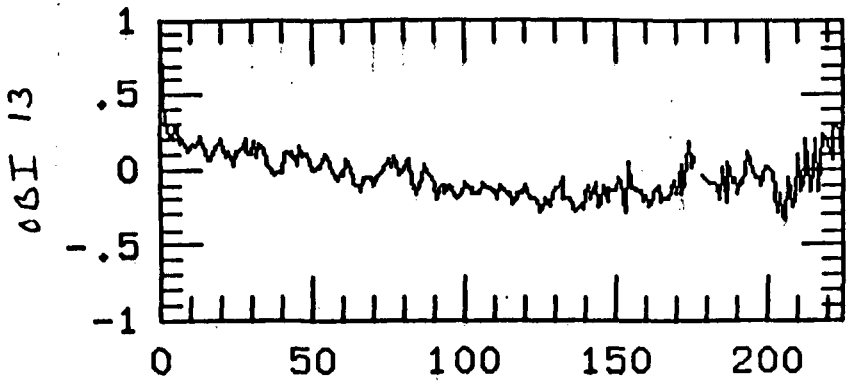

Hard

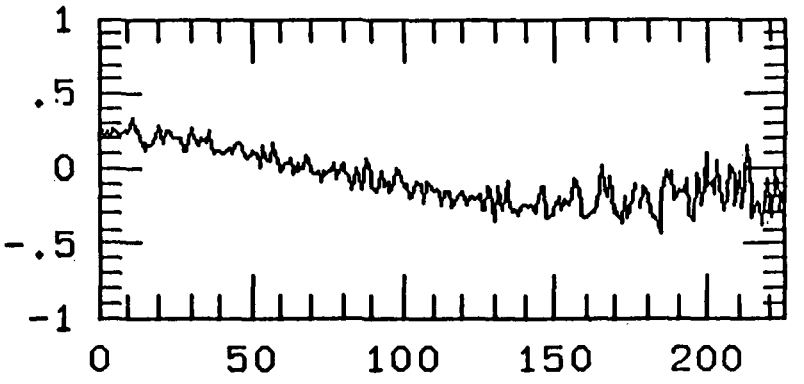

Phase Shift (x 9.20 sec)

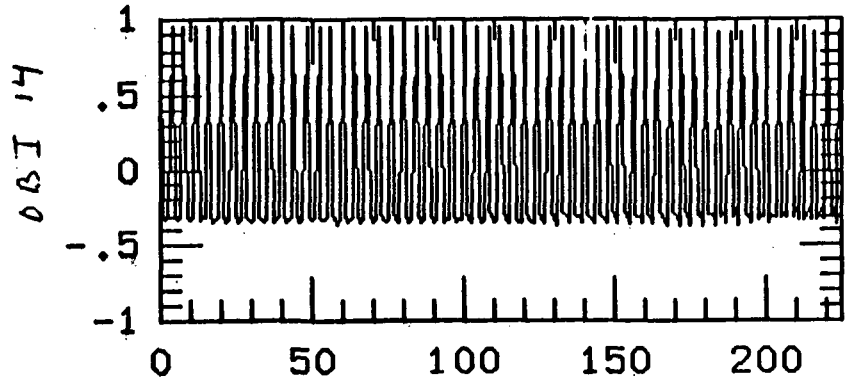

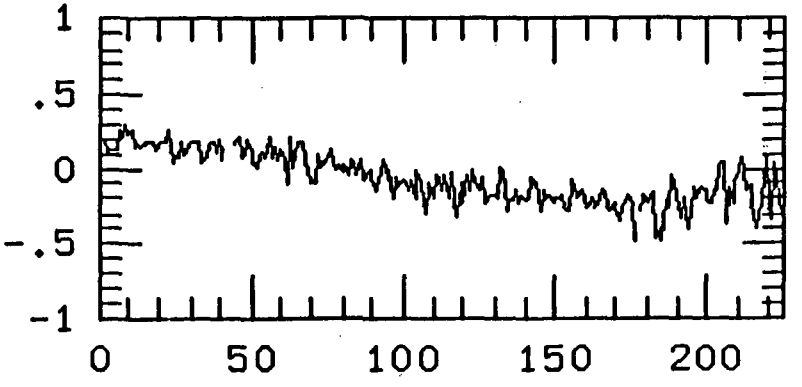

Phase Shift (x 8.7 sec)

References

1. Bevington, P., *Data Reduction and Error Analysis for the Physical Sciences*, Mc-Graw Hill, 1969.

2. Bonnet-Bichaud, J.M. and Mouchet, M., 1987, *Astronomy and Astrophysics*, **188**, 89.

3. Ishida, M., Silber, A., Bradt, H., Remillard, R., Makishima, K., Ohashi, T., 1991, *Astrophysical Journal*, **367**, 270.

4. Lamb, D.Q. 1985, Cataclysmic Variables and Low-Mass X-Ray Binaries, ed. Lamb, D. Q. and Patterson, J. (Dordrecht:Reidel), p. 179.

5. Liebert, J. and Stockman, H. S. 1985, Cataclysmic Variables and Low-Mass X-Ray Binaries, ed. Lamb, D. Q. and Patterson, J. (Dordrecht:Reidel), p. 151.

6. Mason, P.A., Liebert, J. and Schmidt, G. D. 1989, *Astrophysical Journal*, **346**, 941.

7. Press, W., Flannery, B., Teukolsky, S., and Vetterling, W., *Numerical Recipes in C*, Cambridge University Press, 1988.

8. Remillard, R., Bradt, H., McClintlock, J. E., Patterson, J., Roberts, W., Schwartz, D.A., and Tapia, S., 1986, ,*Astrophysical Journal*, **302**, L11.

9. Schraeder, C.R., Remillard, R., Silber, A., McClintlock, J.e., and Lamb, D.Q., 1988, *A Decade of UV Astronomy with the IUE satellite*, ESA SP-281, Vol I, p. 137.

10. Silber, A., Bradt, H., Ishida, M., Ohashi, T., and Remillard, R., 1992 preprint.

11. Stellingwerf, R.F., 1978, *Astrophysical Journal*, **224**, 953.

12. Stockman,H. S., Schmidt,G.D., and Lamb, D.Q., 1988, *Astrophysical Journal*, **332**, 282.

13. Trumper, J., 1983, *Adv. Space Res.*, Vol 2, No 4, pp241-249.